

Hydrodynamics in the pits of Borssele and Hansweert

Data-analysis and Delft3D-FM modeling



Hydrodynamics in the pits of Borssele and Hansweert

Data-analysis and Delft3D-FM modeling

Mick van der Wegen
Reinier Schrijvershof
Ana Colina Alonso
Yorick Broekema
Wouter Kranenburg
Bas Huisman

1210301-015

Title

Hydrodynamics in the pits of Borssele and Hansweert

Project

1210301-015

Attribute

1210301-015-ZKS-0007

Pages

37

Classification

(n.v.t.) until

Keywords

Secondary currents, density flow, gravitational circulation, Western Scheldt

Samenvatting

Binnen het kader van een vergunningsaanvraag voor het storten van baggerspecie in de diepe putten van de Westerschelde heeft de Vlaams Nederlandse Schelde Commissie (VNSC) Deltares gevraagd de sedimentdynamica in de putten te onderzoeken. Deze studie richt zich daarbij op de 3D stroompatronen in twee diepe putten nabij Borssele en Hansweert middels een data-analyse en modelsimulaties.

Zowel metingen als 3D modellering tonen het bestaan van gravitatiecirculatie processen in de hoofd- en secundaire stroomrichting. De secundaire stroming staat haaks op de hoofdrichting en toont absolute snelheden met een orde grootte van 10% van de stroming bij maximum eb en vloed. Meerdere circulatiecellen kunnen dwars op de diepe putten ontstaan. Sommigen ervan veranderen van richting tussen eb en vloed, terwijl anderen hun richting behouden.

Model simulaties tonen dat de secundaire stroming in de putten wordt veroorzaakt door relatief kleine zoutgradiënten. De waargenomen stroming kan dus niet enkel worden verklaard met de klassieke bochtstroming theorie. Uit een grove schaalanalyse van de verschillende termen in de laterale momentum vergelijking blijkt dat de circulatie patronen waarschijnlijk hoofdzakelijk worden gedreven door de baroclinische druk gradiënten, advectieve versnelling en door wrijving. Het waarnemen van zoutgradiënten in toekomstige meetcampagnes zou zeer waardevol zijn om het 3D model in termen van saliniteit te valideren.

De secundaire stroming heeft waarschijnlijk geen grote impact op de omvang van het sedimenttransport, gezien de snelheden ervan (max.~0.3 m/s) beperkt zijn vergeleken met de stroomsnelheden in de hoofdrichting (max.~2 m/s). De secundaire stroming kan echter wel bijdragen aan het mengen van gesuspendeerd sediment in de waterkolom. Daarnaast kan de richting van het bodemtransport worden beïnvloed door de secundaire circulatie. Toekomstige studies zullen in detail ingaan op de invloed van de 3D dynamiek op het sedimenttransport.

Summary

The Vlaams Nederlandse Schelde Commissie (VNSC) asked Deltares to assess sediment transport dynamics in deep pits of the Western Scheldt within the framework of a new permission trajectory for dredging disposal in these pits. As a part of this large investigation, this study investigates 3D-flow patterns in two Western Scheldt pits near Borssele and Hansweert by analysis of field data and numerical model simulations.

Observations and 3D modeling with Delft3D FM show the existence of gravitational circulation processes apparent in the main flow direction and secondary circulation flow perpendicular to the main flow direction with magnitudes of about 10% of the main flow at ebb and flood. Multiple circulation cells may exist in cross-sections across the pits. Some of the circulation cells reverse flow direction from ebb to flood, but some do not.

Title

Hydrodynamics in the pits of Borssele and Hansweert

Project

1210301-015

Attribute

1210301-015-ZKS-0007

Pages

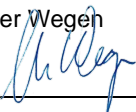


37

Classification

(n.v.t.) until

Model results show that small salinity gradients are the main drivers of the secondary flows in the pits. The observed secondary flows thus cannot be explained by classical river bend flow. A rough scaling analysis of the different terms in the lateral momentum equation shows that the driving mechanisms of the circulation patterns probably consist of the baroclinic pressure gradient, advective acceleration and friction. Including salinity in future transect measurements would provide valuable data to validate the 3D model in terms of salinity.

The secondary flow patterns probably do not have a large impact on the sediment transport magnitude, since the secondary flows (max.~0.3 m/s) remain small compared to the main flows (max.~2 m/s). However, the secondary flows may have an impact by enhancing the mixing of suspended sediments in the water column. Also, the direction of the sediment bedload transport will be affected by the secondary circulations. Future studies on sediment transport in a 3D setting will reveal in more detail the impact 3D flow dynamics may have on sediment transport.

Versie	Datum	Auteur	Paraaf	Review	Paraaf	Goedkeuring	Paraaf
0.1	Nov. 2019	M. van der Wegen		J. Vroom		F. Hoozemans	
	Draft						
1.0	Jan. 2021	M. van der Wegen		J. Vroom		T. Segeren	
	Final						

Status

Final

Content

1	Introduction	1
1.1	Background	1
1.2	Study objective and research questions	1
1.3	Report structure	2
2	Data-analysis flow	3
2.1	Introduction	3
2.2	Description of the Borssele measurement campaign	3
2.2.1	Transects	3
2.2.2	Settings of the measurement equipment	4
2.2.3	Borssele pit morphology	4
2.3	Measurement campaign Hansweert	5
2.3.1	Transects	5
2.4	Borssele pit results	6
2.4.1	Depth-averaged flow	6
2.4.2	Flow distribution over the vertical	10
2.5	Hansweert Pit results	13
2.5.1	Depth-averaged velocities	13
2.5.2	Flow distribution over the vertical	14
3	Modelling study with Delft3D Flexible Mesh	17
3.1	Introduction	17
3.2	Model set-up	17
3.2.1	Grid	17
3.2.2	Boundary conditions	18
3.2.3	Bathymetry	18
3.2.4	Wind forcing	18
3.2.5	Bottom roughness	18
3.2.6	Hydrodynamic spin-up	18
3.3	Validation	19
3.3.1	Water levels and depth-averaged flow	19
3.3.2	Vertical velocity profiles	21
3.3.3	Comparison between the model runs	23
3.4	Modelling results	26
3.4.1	3D flow patterns: secondary flow	26
3.4.2	Process analysis	29
4	Discussion	31
4.1	Comparison to traditional river bend flow	31
4.2	Analysis of governing processes	32
4.3	Possible impact on sediment transport	33
5	Conclusions	35
6	Referenties	37

Appendices

A	Validation additional transects Borssele	A-1
B	Velocity profile validation over depth	B-1

1 Introduction

1.1 Background

To safeguard the access to the Port of Antwerp dredging takes place in the Western Scheldt on a regular basis. The dredging activities mainly consist of limiting the height of the sills between subsequent bends in the main access channel since these are the shallowest part of the access channel. In addition, current policy aims at preserving the dredged material within the same part of the Western Scheldt. To prevent quick re-sedimentation of the sills, the dredged material is typically placed at low-energy locations, such as shoals or side-channels, or at eroding edges of the main channel (e.g. at the eastern embankment of the Gat van Ossensisse). A new strategy to place dredged sediment from the sill in the deepest parts of the channels (i.e. the access channel bends, also referred to as 'pits') is proposed, because of the lower impact on the intertidal environment (i.e. placing sediment in a less ecologically sensitive high-energy environment). Over time, sediment erodes from these pits while the sills accumulate sediments again requiring another round of dredging. It is important to understand the processes responsible for this morphological response. How fast is the sediment eroding from the pits? What processes are responsible for this? What are best dumping locations to lengthen dredging intervals?

Within the framework of a new permission trajectory for sediment deposition in deeper parts of the Western Scheldt, the Vlaams Nederlandse Schelde Commissie (VNSC) asked Deltares to contribute to the knowledge base on the hydrodynamic and morphological impacts of dredged sediment disposal in the deep pits of the Western Scheldt in support of the upcoming application for a dredging license in 2020. This study aims at obtaining a solid understanding of the 3D hydrodynamic processes in the deep pits.

The study provides a basis for evaluation of the morphological impacts of the dredged sediment disposal strategy and quantification of the expected dredging volumes. The larger framework of this study encompasses an investigation of the transport pathways of sediment in the deep pits of the Western Scheldt. A major question thus relates to the potential impact of the observed and modeled secondary flow on the sediment transports. Earlier modeling studies showed that 2D models were not able to predict the transport of deposited sediment from the pits (Deltares, 2018). The focus of the current study is thus on 3D flow patterns, whereas future studies will focus on 3D sediment transports.

1.2 Study objective and research questions

The objective of this study is to investigate prevailing 3D flow patterns in the pits of Borssele and Hansweert in the Western Scheldt using numerical modelling and in-situ measurements of hydrodynamic conditions. This hydrodynamic study provides a basis for the evaluation of the morphological impacts of the dredged sediment disposal strategy and quantification of the expected dredging volumes.

The following research questions are formulated:

- What are the prevailing 3D flow patterns in the pits of Borssele and Hansweert?
- Can these flow patterns be modeled by a 3D hydrodynamic model (Delft3D FM)?
- What are the processes responsible for the 3D flow patterns?
- What are the potential implications of these flow patterns on the transport of sediment deposited in the pits by dredging activities?

1.3 Report structure

This report is structured as follows. First, we will focus on a close analysis of measurements taken by Rijkswaterstaat (Schrijver M. and J van het Westende,, Rijkswaterstaat CIV, personal communication 2018) on the 3D flow patterns in the pits. Secondly, we validate a 3D flow model of the Western Scheldt (Delft3D FM) against the observations. Thirdly, we perform a sensitivity analysis to derive the governing mechanisms that drive the 3D circulation patterns. Finally, we discuss the model outcomes in the framework of the potential implications for sediment transport in the Western Scheldt pits.

2 Data-analysis flow

2.1 Introduction

The analysis in this chapter aims to describe and characterize the flow patterns in the deep pits of Borssele and Hansweert. This is done via an analysis of flow measurements (ADCP) taken in both pits. The central question reads: What are the prevailing 3D flow patterns in the pits of Borssele and Hansweert?

2.2 Description of the Borssele measurement campaign

The hydrodynamic measurements were carried out on November 28th, 2011, in the Borssele pit. The plan for this field campaign was made based on a test measurement on July 22nd, 2011 also in the Borssele pit. A 13-hour field campaign measuring the flow conditions was carried out on November 28th with a sailing ADCP on a ship. Schrijver and Van het Westende (2011) describe these measurements and shows measured hydrodynamic information.

2.2.1 Transects

Four transects were measured during the November 28th field campaign by means of an Acoustic Doppler Current Profiler (ADCP) mounted under the vessel "MS Kaloo". The four transects were positioned across the Borssele pit. The start and end coordinates are given in Table 2.1.

Table 2.1 Measurement transects coordinates (Rijksdriehoeksstelsel).

Raai	X ₁	Y ₁	X ₂	Y ₂
Raai 1	38.206	382.185	38.668	382.650
Raai 2	38.075	382.337	38.536	382.805
Raai 3	37.948	382.474	38.409	382.943
Raai 4	38.080	382.920	38.660	382.365

Figure 2.1 shows the locations of the transects on an aerial plot (Google Earth). Three transects are directed laterally from South-West to North-East and one transect is directed along the pit from North-West to South-East. The transects are located close to the intake and outflow of the Borssele nuclear power plant. The breakwaters and flow patterns associated with the intake/outflow may affect the flow patterns in the Borssele pit by induced turbulence and temperature anomalies. For example, Figure 2.1 shows clearly a lighter colored area at the transect locations.

The measurements started on November 28th at 05:51 hrs at point A' and ended at 18:54. The transects were made in the following order:

A' → A → B → B' → C' → C → D → D' → A'

The flow measurements were carried out during a period of 13 hours and 3 minutes where each transect was measured 34 times. The measurement of a complete set of transects (transect 1 to 4) took about 20 to 25 minutes.



Figure 2.1 Location of the measurements in the Pit of Borssele.

2.2.2 Settings of the measurement equipment

The measurement equipment used was a Teledyne RD Instruments 600 kHz ADCP. The equipment was set in such a way that the flow was measured in a maximum of 75 depth cells (bins) of 1 meter. The equipment allows to measure flow till about 94 % of the flow depth. The equipment was mounted under the vessel so that the minimum water depth of the measurements was about 3 m. The ADCP flow data was processed by Rijkswaterstaat. The processed data were delivered as text files with flow magnitude and direction for each transect. A text file with depth-averaged flow was also delivered.

2.2.3 Borssele pit morphology

Figure 2.2 shows the bathymetry at the transect locations, which is interpolated from measurement transects from 2011 Rijkswaterstaat Vaklodgingen. The transects are positioned across the deepest part of the pit. The deepest point in the Borssele pit is about -60m NAP. The pit's shape resembles an elongated ellipse with the longest axis in the main flow direction. The southwesterly channel slope is milder than the northeasterly slope. The pit can be considered as part of a channel bend where the northeasterly channel slope forms the outer bend.

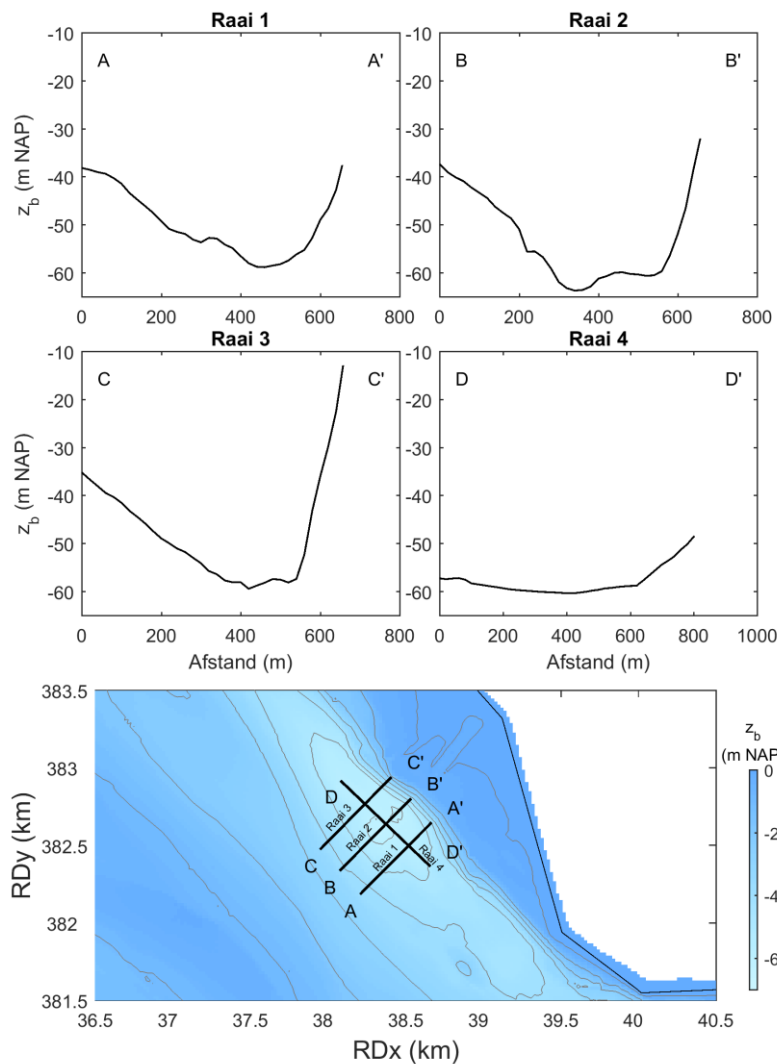


Figure 2.2 Positioning of the transects (lower panel) and bathymetry at the transects (top panels). The bathymetry originates from 2011 Rijkswaterstaat Vaklodgingen.

2.3 Measurement campaign Hansweert

In December 2018 similar measurements were carried out in the deep pit of Hansweert. The currents during ebb were measured on December 14th (about 2 days before neap tide) and the flood currents were measured on December 20th (about 2 days before spring tide). The set-up and results of the measurements are described by Rijkswaterstaat CIV (Personal communication, 2018).

2.3.1 Transects

Two transects were measured with an ADCP: one straight transect across the channel (in SE direction) and one curved transect along the channel bend (Figure 2.3). The coordinates of the start and end points of the transects are shown in Table 2.2.

Table 2.2: Measurement transects coordinates

Transect	X_1	Y_1	X_2	X_2
Hansweert 1: E-E'	58.592	384.385	58.437	383.811
Hansweert 2: F-F'	59.454	383.581	57.495	383.987

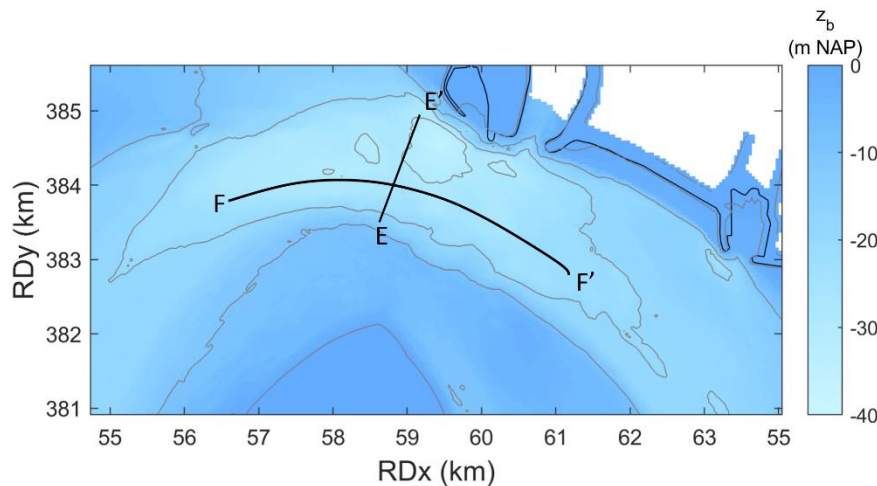


Figure 2.3: Positioning of the measured transects in the pit of Hansweert.

The measurements started on December 14th 07:03h at the eastern side of transect F-F'. The duration of the measurements in this transect was 8 minutes on average. Measuring the shorter transect E-E' took about 2 minutes. The transects were measured 17 times on December 14, and 15 times on December 20th.

2.4 Borssele pit results

2.4.1 Depth-averaged flow

Figure 2.4 shows a timeseries of the depth averaged flow conditions in the Borssele pit for all measurements. The depth-averaged values (gray dots) originate from different waterdepths (along the transects) so that one can observe considerable variation in flow velocity. The blue dots represent the averaged value per transect. The red line shows the depth-averaged flow on the basis of averaging over the 4 transects. The figure also shows the water level at the Borssele water level observation station. The tide at November 28th is about halfway the neap-spring tidal period.

The measurements started during ebb when the flow direction was in northwesterly direction ($\sim 320^\circ$; Figure 2.4). The peak flood flow was in southeasterly direction. ($\sim 140^\circ$). The flow direction in the Borssele pit is strongly bimodal (only two main directions). The depth-averaged maximum ebb flow is about 1.3 m/s (gray dots). The maximum flood flow is considerably larger; almost 2 m/s. The duration of the ebb phase is longer than the flood phase. This implies that the Borssele pit is clearly flood dominant in terms of peak flows.

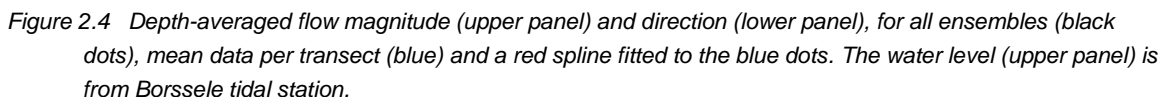
Representing the spatial distribution of the depth-averaged flow, Figure 2.5 and Figure 2.6 show the maximum ebb flow and the maximum flood flow in a vector plot, respectively. During

maximum ebb the largest depth-averaged flows are reached near the southeasterly border of the measured area. The flow decreases in northeasterly direction towards the shore. The decrease is almost linear in relation to the distance to the shore and is about 1 m/s along the transects. The transect parallel to the primary flow direction (transect DD') shows that the flow decelerates towards the deepest point in the pit after which it accelerates again. The variation along this transect is about 0.3 m/s.

Compared to peak ebb flow, the peak flood flow remains quite uniform along the cross-transects (transects 1-3), albeit velocities decrease fast near the northern channel slope. The maximum flow velocity occurs in the central, deepest part of the pit. The distribution across the parallel transect (4) is different from peak ebb flow in the sense that the highest velocities are located in the central part of the transect, while the depth-averaged flow decreases longitudinally towards the edges of the transect.

The spatial variation in flow velocity magnitude is further illustrated by Figure 2.7, showing the relative flow distribution across parallel transect (4) for some individual transect measurements around the moment of peak ebb flow (Figure 2.7a) and peak flood flow (Figure 2.7b). The depth-averaged flow has a maximum value at the pit edges during ebb flow and a minimum value just upstream (south easterly direction) of the deepest part of the pit. During peak flood this relationship is redirected; the depth-averaged flow has a minimum value at the edges and a maximum value just upstream (in northwesterly direction) of the deepest part of the pit.

The different behaviour during ebb and flood flow relates to tidal asymmetry. Peak ebb flow occurs at a lower water level (and smaller cross-section) than peak flood flow (see Figure 2.4). Apart from the small river flow, ebb and flood volumes should be equal reflected by an ebb duration that is longer than the flood duration.



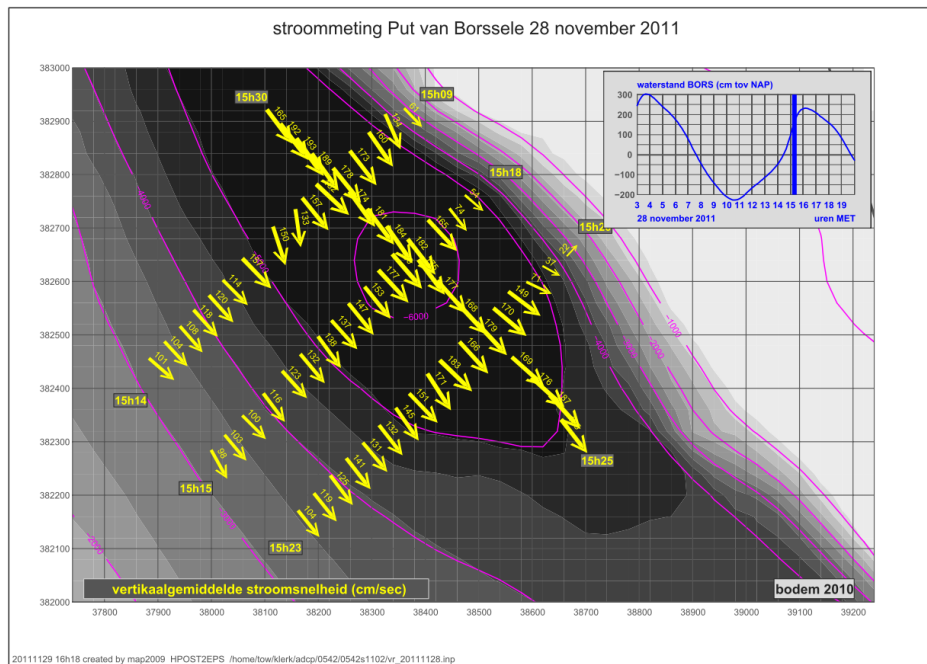


Figure 2.6 Vector plot of depth-averaged peak flood flow (by Rijkswaterstaat).

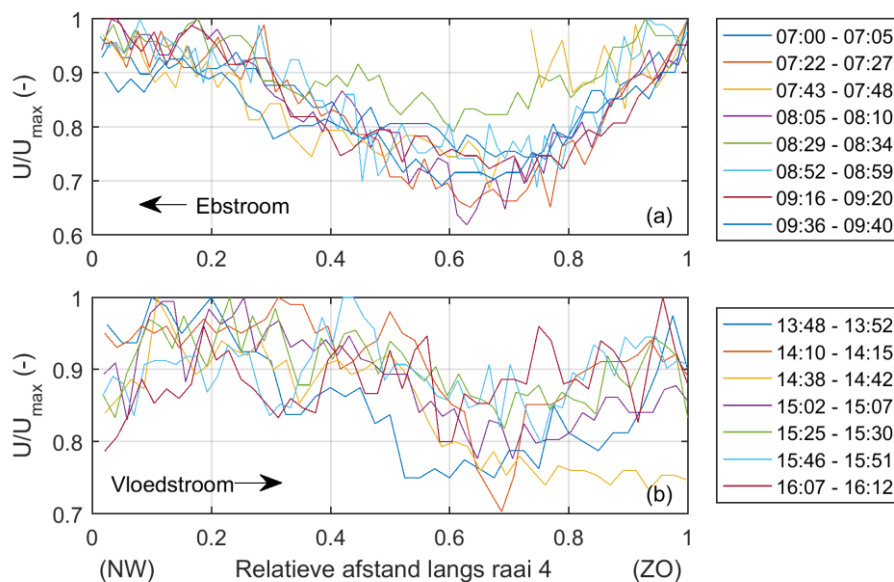


Figure 2.7 Distribution of flow velocity along transect 4 (D-D') for different points in time during ebb flow (upper panel) and during flood flow (lower panel). The flow velocity is normalised by the maximum value along the transect.

2.4.2 Flow distribution over the vertical

Figure 2.8 and Figure 2.9 show the distribution of the flow velocity and direction over the transects and over the vertical. The colorscale was set a maximum value of 1.3 m/s and contourlines indicate the depth with equal velocities.

At peak ebb, the flow direction is quite homogenous over the transects, despite a more south-westwardly directed flow at the northern edge. The flow magnitude is largest at the surface and smallest near the bed. Besides there is considerable variation of flow and depth across the transects perpendicular to the main flow (transects AA' to CC'). Earlier we showed that the depth averaged velocity varies across the pit, with lower depth averaged flow velocities in the deepest part. Now we conclude that this is mainly due to low velocities in the deeper parts of the pit, while surface velocities remain quite uniform across the transect. Figure 2.9 shows that peak flood flows are larger than peak ebb flows. Again, the flow direction is quite uniform across the transects (AA' to CC') apart from an area close to the northern shore.

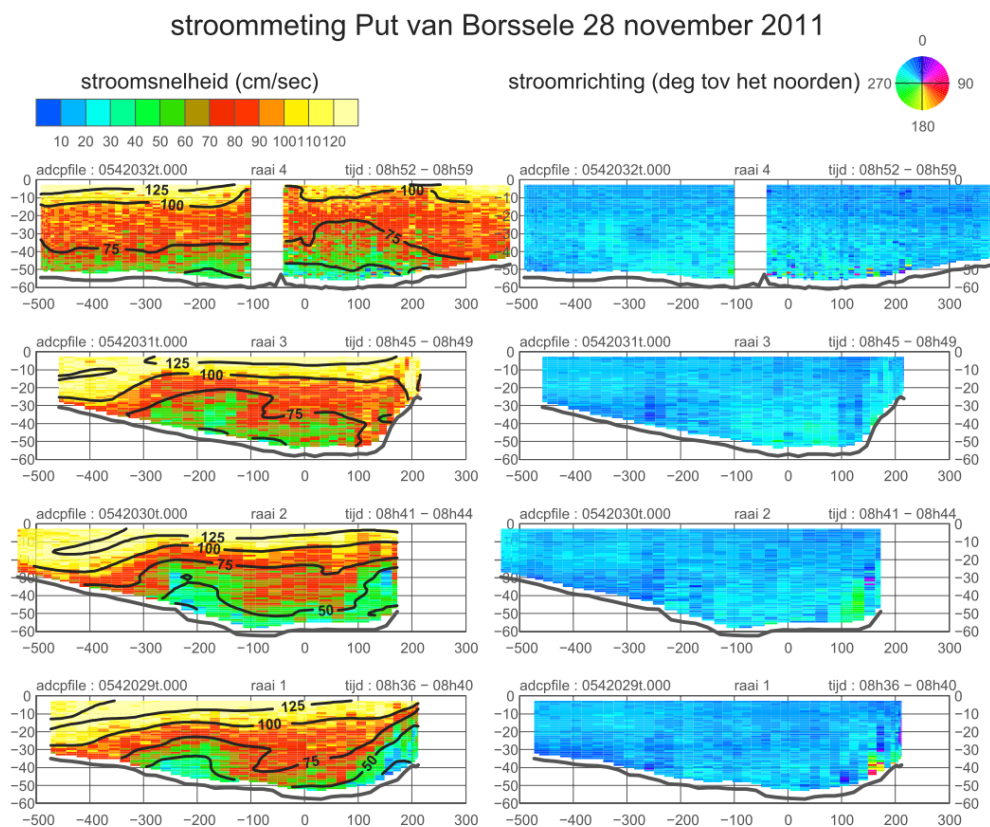


Figure 2.8 Flow velocity (left) and direction (right) during maximum ebb, for transects AA'-DD'

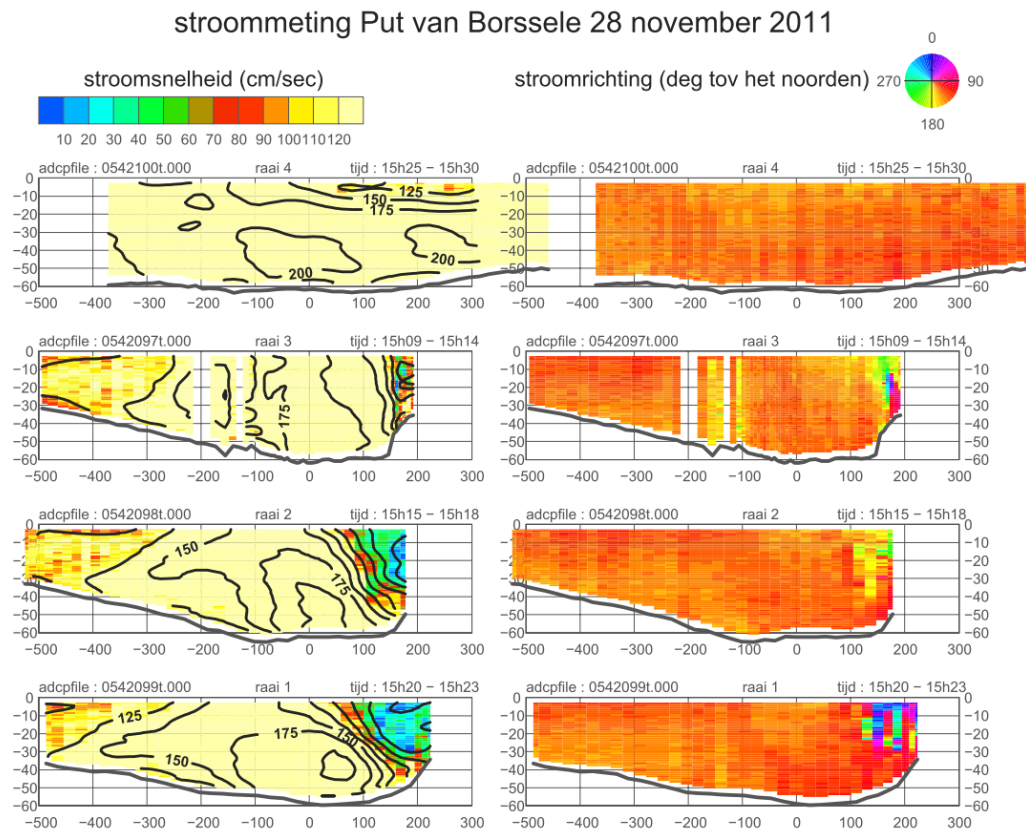


Figure 2.9 Flow velocity (left) and direction (right) during maximum flood, for all transects

Figure 2.10 and Figure 2.11 show different peak ebb and flood flow characteristics at the 3 locations where the transects intersect with the alongshore transect. Unlike the ebb flow velocities, the maximum flood velocities occur sub-watersurface, i.e. the profile is more parabolic. These different velocity profiles are the result of gravitational circulation. Under vertically well mixed conditions small horizontal (salinity driven) density gradients cause a tide-residual current, which is landward near the bed and seaward near the water surface. This results in a stronger (weaker) ebb (flood) flow at the surface and a weaker (stronger) ebb (flood) flow in the lower portions of the water column. This effect will be more pronounced in deeper water.

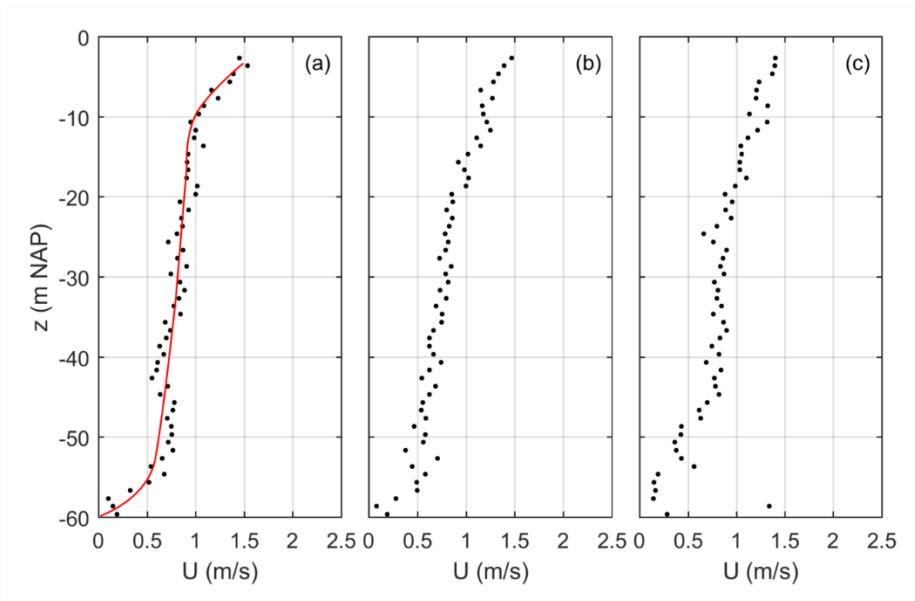


Figure 2.10 Velocity profiles at peak ebb flow at locations where the transects cross.

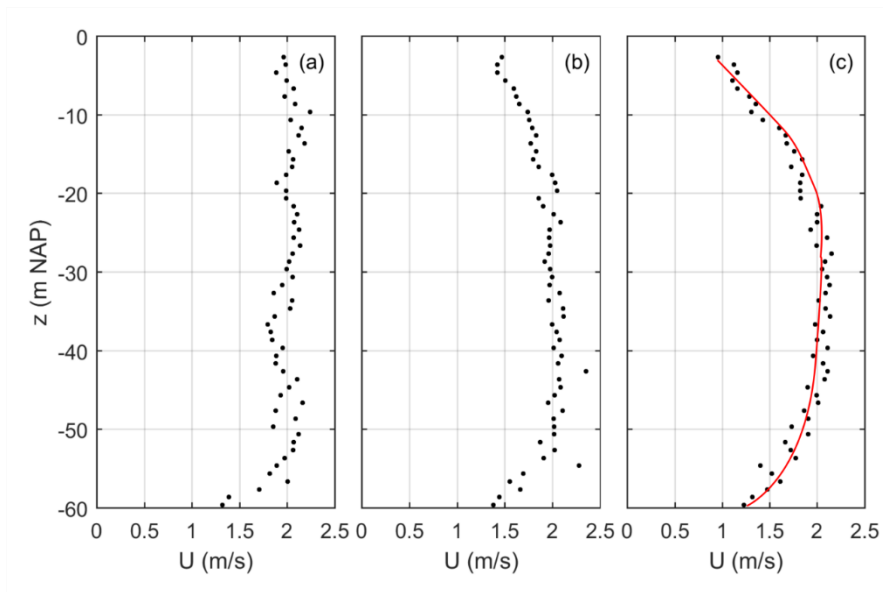


Figure 2.11 Velocity profiles at peak flood flow at locations where the transects cross.

2.5 Hansweert Pit results

2.5.1 Depth-averaged velocities

Similar to the currents at Borssele, the currents at Hansweert have a strong bimodal character, with a rapid transition between flood and ebb. Maximum values of the depth-averaged flow are about 1.3 m/s during ebb and 1.4 m/s during flood. The peak flow asymmetry in this pit is therefore much smaller than in the pit of Borssele.

Figure 2.12 and Figure 2.13 show a map of the depth-averaged currents for maximum ebb and flood. During ebb we find the highest flow velocities along the north part, at the location where the pit is deepest and east part of the bend. During flood, the strongest currents occur in the center part of the channel.

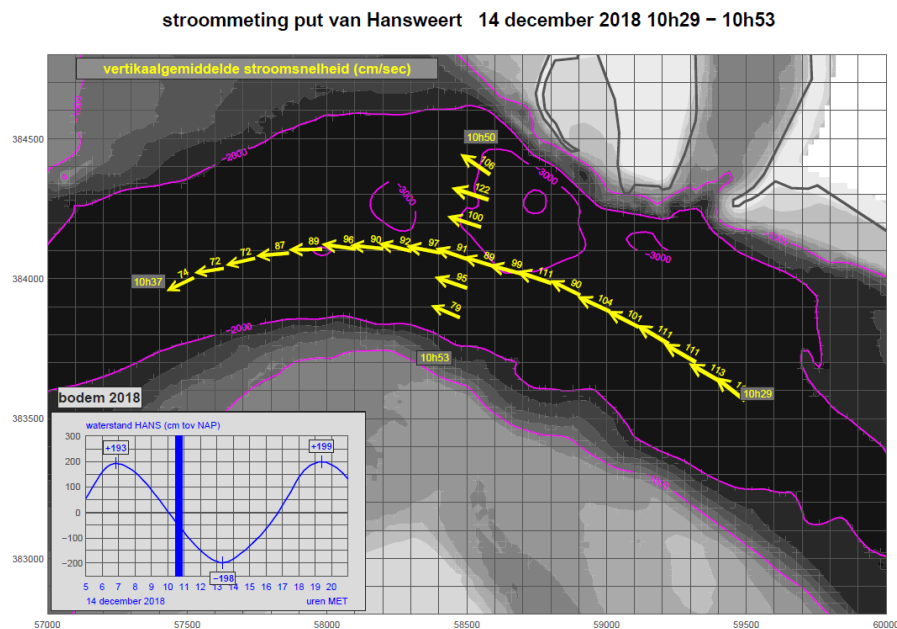


Figure 2.12 Vector plot of depth-averaged peak ebb flow (by Rijkswaterstaat).

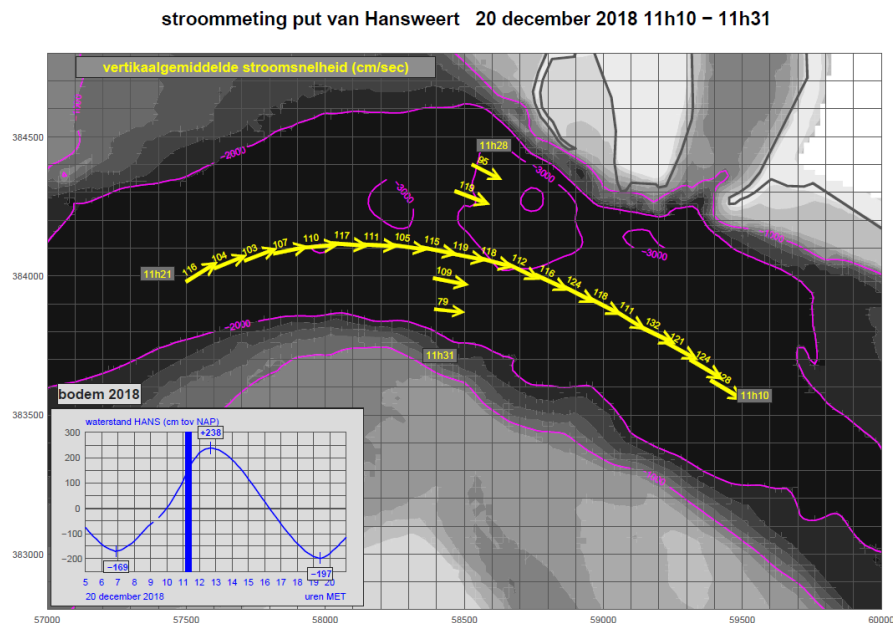


Figure 2.13 Vector plot of depth-averaged peak flood flow (by Rijkswaterstaat).

2.5.2 Flow distribution over the vertical

The vertical distribution of the flow velocities over the transects is shown for maximum ebb and maximum flood velocities in Figure 2.14 and Figure 2.15 respectively. Again, the left figures show the flow magnitude and the right figures indicate the flow direction. The upper panels correspond to transect F-F' along the channel, and the lower to the shorter transect E-E' across the channel (see Figure 2.3 for the exact locations).

Looking at the ebb profiles, the velocity distribution shows many similarities with the profiles found at Borssele. The flow direction is constant over the cross-sections. The highest flow velocities are found in the upper part of the water column, being two to three times larger than the flow velocities near the bed. Also, strong lateral variations are found, since the flow velocities significantly decrease with decreasing distance to the shoal of Ossensisse in the south. Note that at the water surface the flow velocities are much larger than at the channel parallel transect.

The flow field seems to be much more uniform during flood. However, this could also be an effect of the color scale, which has maximum values at 1.3 m/s. Nevertheless, maximum flood flow velocities are found in the central part of the water column, while flow velocities near the bottom and at the surface are in the same order of magnitude. Note that even the flow velocities near the shoal (at the left end of transect 1) are relatively high.

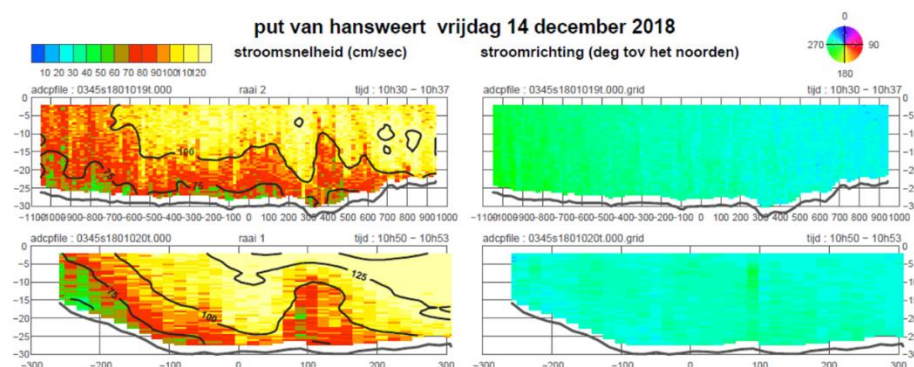


Figure 2.14 Flow velocity (left) and direction (right) during maximum ebb, for both transects

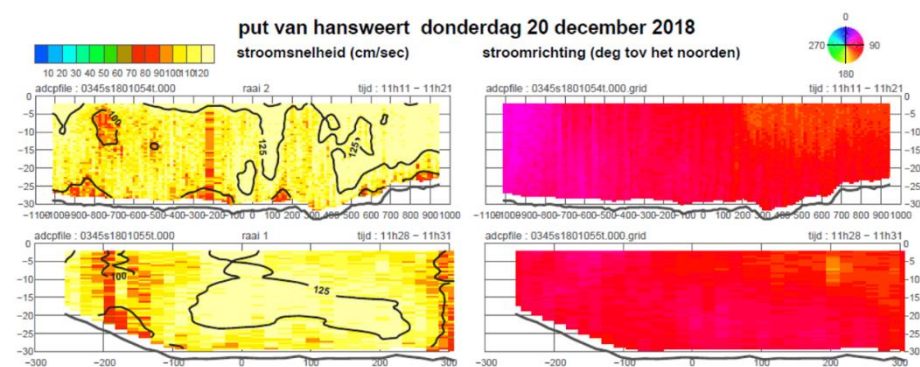


Figure 2.15 Flow velocity (left) and direction (right) during maximum flood, for both transects

3 Modelling study with Delft3D Flexible Mesh

3.1 Introduction

The 3D modeling exercise is undertaken to analyze the processes responsible for the 3D flow circulation patterns observed in the measurements. We applied Delft3DFM since that software allows for a flexible grid refinement covering the pit locations, while maintaining coarser resolutions in the remaining part of the domain. This favors computational efficiency.

3.2 Model set-up

The model set-up is based on the NeVla model as described by Tiessen et al. (2016). In order to compare the model results with the ADCP-measurements in Borssele and Hansweert, two scenarios have been established: one for a hindcast of 2011 and one for 2018. Besides, sensitivity runs have been carried out to test the effect of local grid refinements, the amount of sigma layers, salinity and roughness. An overview of the simulations is shown in Table 3.1. The model parameters that differ from the set-up used by Tiessen et al. (2016) are described in this section.

Table 3.1 Model simulations overview

Run	Year	Grid	Nr layers	vertical	Salt included	Bed roughness	Runtime (hr)
2011-01	2011	Fine	20		yes	Regular	780
2011-02	2011	Coarse	20		yes	Regular	426
2011-03	2011	Coarse	8		yes	Regular	147
2011-04	2011	Coarse	8		no	Regular	156
2018-01	2018	Fine	20		yes	Regular	1061
2018-02	2018	Fine	8		yes	Regular	365
2018-03	2018	Coarse	8		yes	Regular	202
2018-04	2018	Coarse	8		yes	Increased	200

3.2.1 Grid

The simulations with the coarse grid make use of the computational grid set-up by Tiessen et al (2016). Additionally, two computations are done including local refinements at Borssele and Hansweert. Figure 3.1 shows part of the computational grid including these refinements.

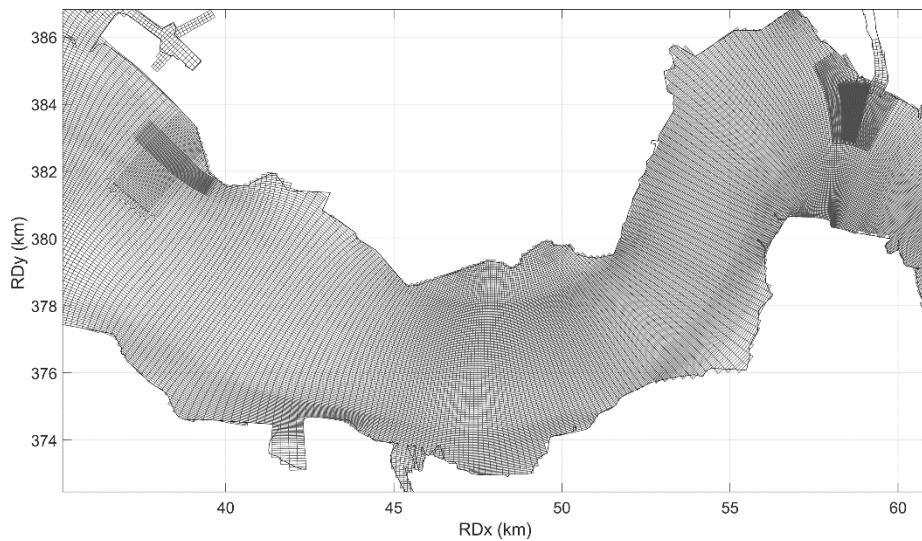


Figure 3.1 Computational grid, including local refinements

3.2.2 Boundary conditions

The boundary conditions for 2011 and 2018 are derived from the DCSM-ZUNO models, versions DCSMv6-ZUNOV4 2011 (including Kalman filter) and DCSMv6_ZUNOV4 2018 (excluding Kalman filter) respectively. At the northern and southern boundaries water levels and perpendicular flow velocities are imposed. At the western offshore boundary, a water level boundary is implemented. At the upstream river boundaries, the river discharge measurements are used.

3.2.3 Bathymetry

The bathymetry of the models is based on the Vaklodingen datasets. For the 2011 model, the entire bathymetry is based on the Vaklodingen data of 2011. For the 2018 model, the bathymetry in the Western Scheldt has been updated with the data of 2018. The offshore bed levels at the North Sea have not been updated, due to an absence of new data. We had to deepen the beach locally to 5m at the northern and southern boundaries, since instabilities occurred because of the wetting and drying at these intertidal areas.

3.2.4 Wind forcing

A spatially uniform wind forcing is implemented, based on the time series of the potential wind at Vlissingen (velocity and direction). This time series is provided by KNMI and has a frequency of 10 minutes.

3.2.5 Bottom roughness

The bottom roughness is parametrized as a spatially varying Manning coefficient. In most simulations, the coefficient derived by Vroom et al. (2015) are used (referred to as regular roughness in Table 3.1). Additionally, one sensitivity simulation is executed with increased roughness values (5% higher over the entire domain).

3.2.6 Hydrodynamic spin-up

In particular the salinity field required a considerable spin-up of about 3 months, implying that the runs started three months earlier than the date of the measurements. This led to considerable computational time ranging from 780 hours (~32 days) for the model with refined horizontal mesh in the pits and 20 sigma layers to 147 hours (~6 days) for the model with a uniform coarse horizontal mesh and 8 sigma layers, see Table 3.1.

3.3 Validation

In this section the (hindcast) skill of the model is discussed. We compare the water levels, depth-averaged velocities and depth integrated velocity profiles with measured data. Besides, a comparison between the model set-ups is presented.

3.3.1 Water levels and depth-averaged flow

Figure 3.2 and Figure 3.3 show the measured and predicted water levels and flow velocities for the periods and locations at which the ADCP measurements took place. The modelled water level elevation at Borssele matches the measured water levels, indicating a satisfactory performance of the model in this regard. The depth-averaged velocities also coincide well with the measurements. The modelled flow at Hansweert shows larger deviations from the measured flow. The model tends to overestimate the water level (especially at high water) and also slightly overestimates the depth-averaged flow velocities. These deviations are observed in all model simulations, regardless of the grid size. Therefore, sensitivity computations with increased manning coefficients were executed. This is discussed in Section 3.3.3.

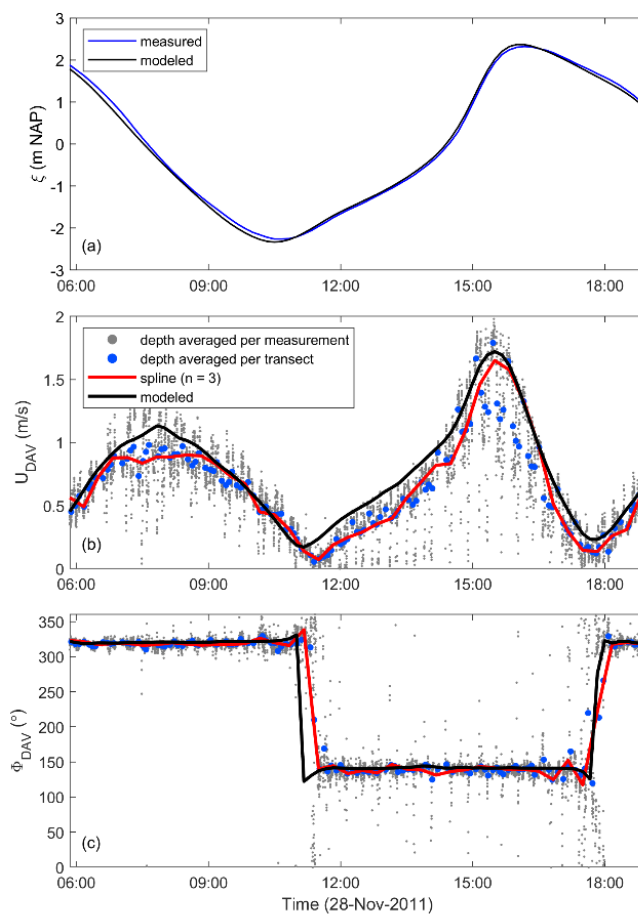


Figure 3.2 Validation of the water levels and depth averaged velocities in Borssele

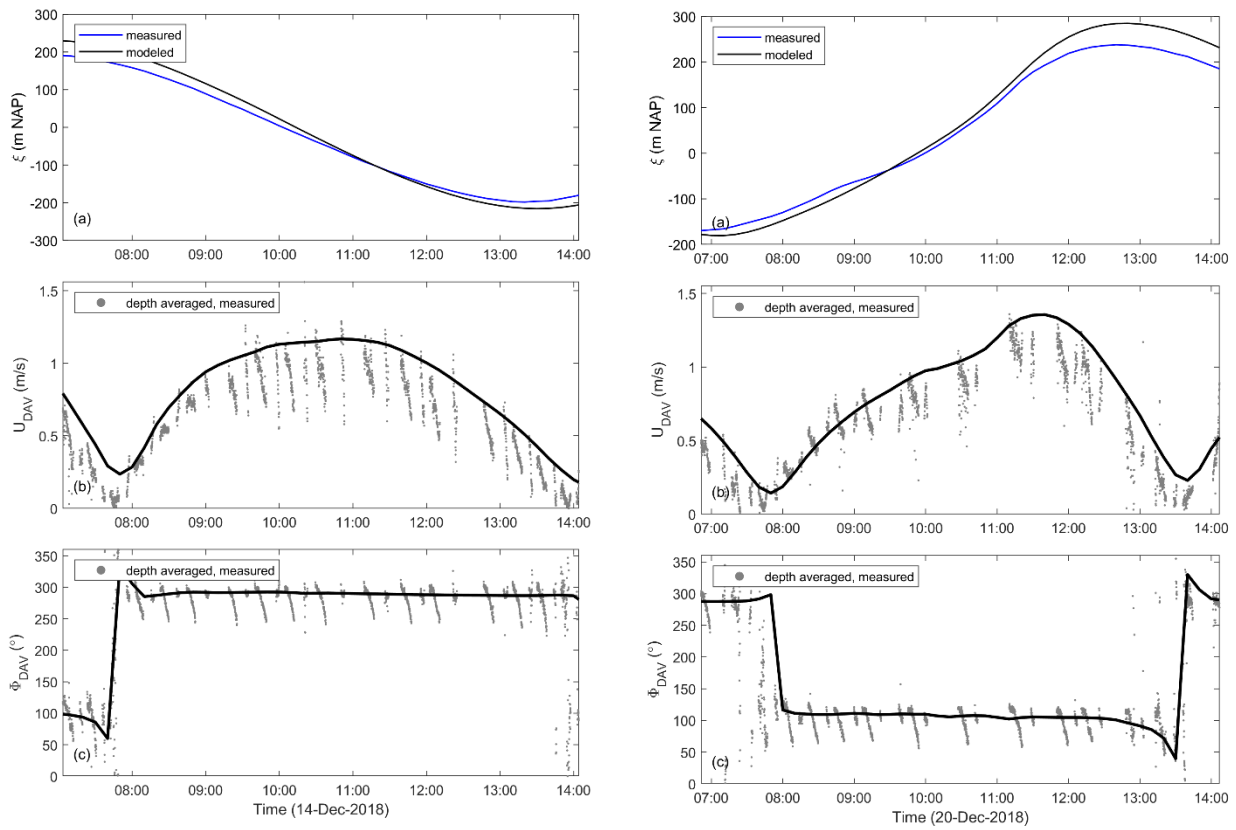


Figure 3.3 Validation of the water levels and depth averaged velocities in Hansweert (left for ebb and right for flood)

3.3.2 Vertical velocity profiles

The 3D model results (with grid refinement and 20 layers) are compared to vertical velocity profiles along the transects. We consider the flow at each point separated into a primary flow in m-direction and a secondary, circular flow in n-direction such that the depth-averaged secondary flow equals 0, while the primary flow m-direction is perpendicular to the n-flow direction. This implies that the primary flow direction slightly varies across the transects.

Figure 3.4 and Figure 3.5 show the velocities in m- and n-direction for maximum flood and maximum ebb at transect 2 (B-B') in Borssele. Appendix A shows the measured and modeled AA' and CC' transects. Appendix B shows a comparison between model results and measurements per location in the BB' transect. The simulated flow patterns coincide well with the measurements. The model grasps the flow velocities, directions and 3D flow patterns. The measured and modeled bathymetries generally have the same shape, but also deviate. We attribute this to the difference in timing of the Vaklodingen used for the model bathymetry compared to the timing of the measured transects. Apart from interpolation errors and measurement accuracy, the difference may thus be interpreted as an indication for morphodynamic development within (maximum) a year.

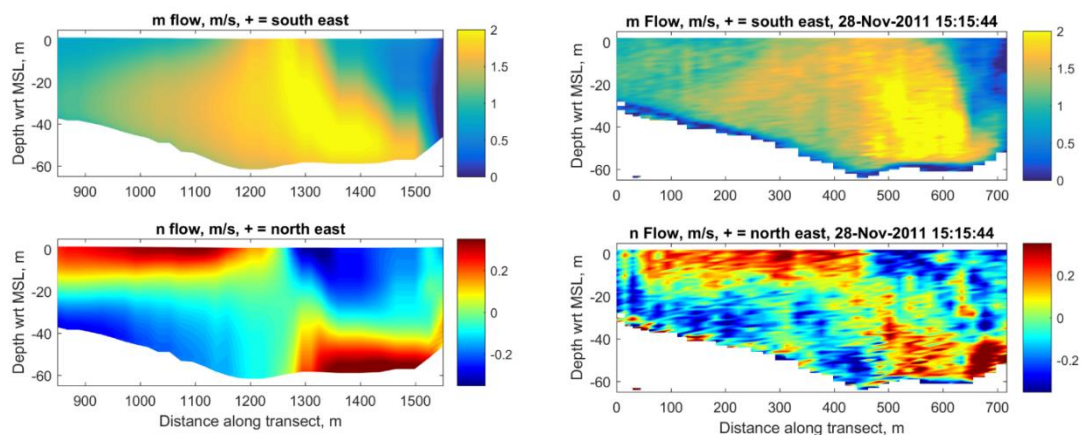


Figure 3.4 Transect B-B' during flood, model results (left) and data (right).

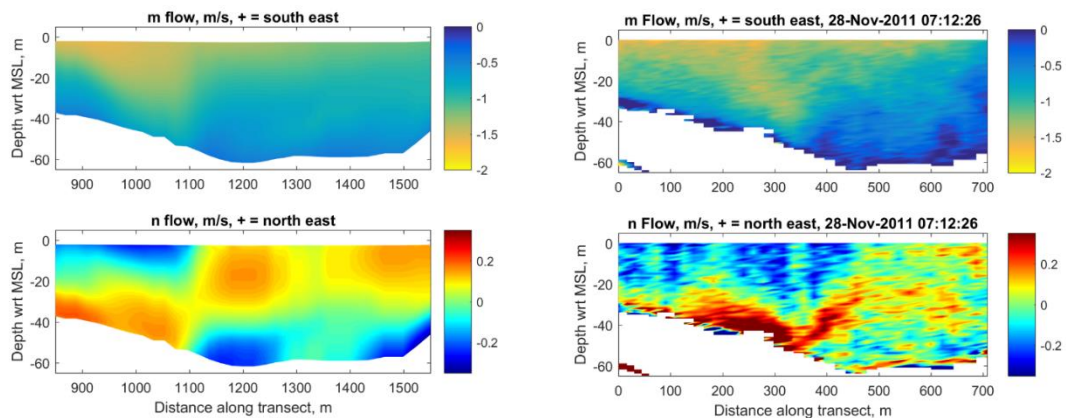


Figure 3.5 Transect B-B' during ebb, model results (left) and data (right).

The same comparison between model results and data has been executed for the flow in the pit of Hansweert (see Figure 3.6 and Figure 3.7). Again, the model is able to reproduce the general flow patterns, although some differences can be observed for maximum ebb (at the lower left edge of cross section E-E'). These are mostly induced by measurement errors of the ADCP near the bed, as the measurements taken close to the bed show flow patterns that deviate strongly from the layers above. Since the n-direction is defined such that the net secondary flow over the vertical equals 0, an error in one of the measuring bins can lead to a different pattern. Analysis of the ADCP data has shown that this is the case for the bins at the lower left edge of cross section E-E' during ebb (lower left panel in Figure 3.7). Therefore, it is advised to exclude this data before performing the directional analysis in the future.

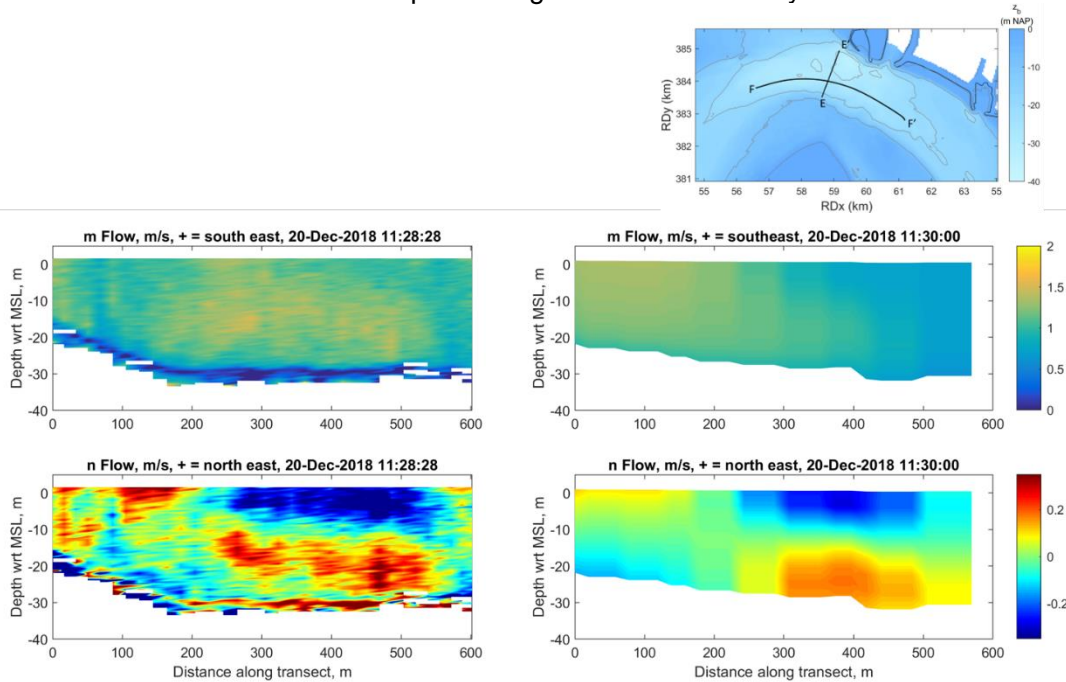


Figure 3.6 Transect E-E' during flood, data (left) and model results (right).

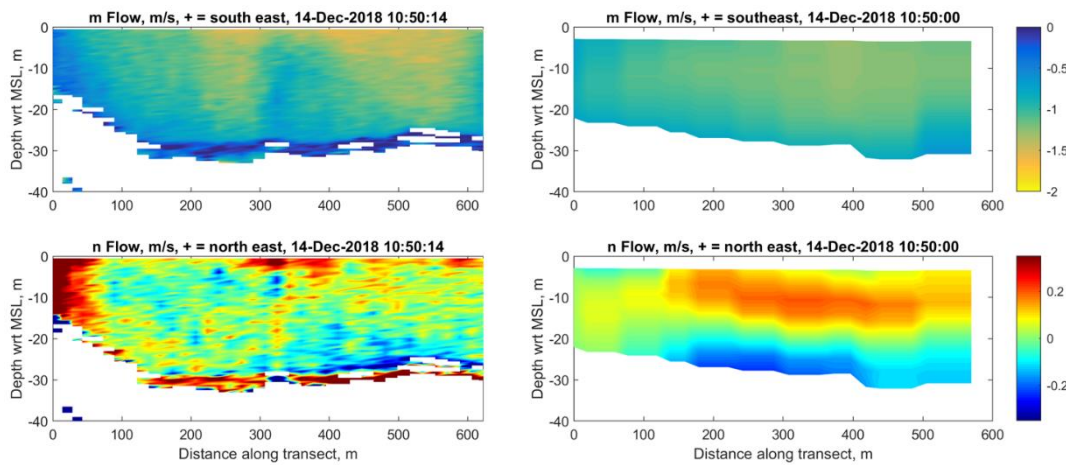


Figure 3.7 Transect E-E' during ebb, data (left) and model results (right).

Figure 3.8 shows the direction of the main flow defined by the direction that gives a zero depth-averaged secondary flow. Measured and modelled directions are similar, albeit that the measured directions show more variations over the transect. This is probably due to measured,

velocities that show irregular behaviour near the bed (see for example Figure 3.7 lower left panel) probably due to measurement inaccuracies that are known to be largest at more than 94% of the water depth.

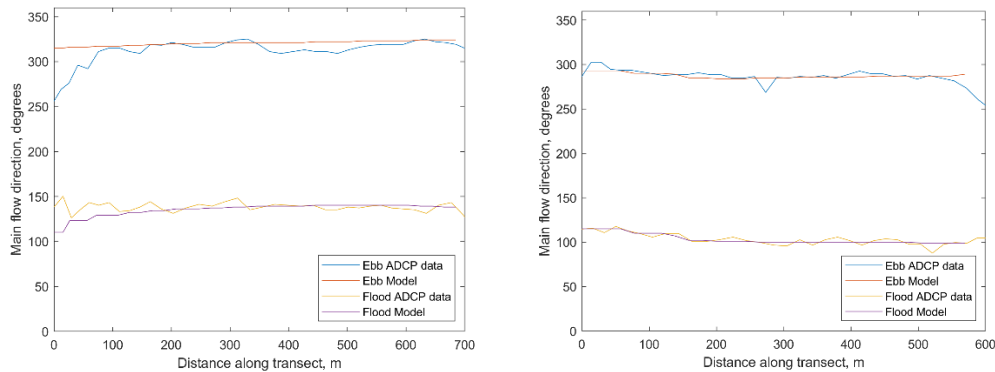


Figure 3.8 Direction of main flow for Borssele and Hansweert at ebb and flood and for observation and model results

3.3.3 Comparison between the model runs

Depending on the model settings, the computational times may vary significantly. The most detailed settings (fine grid, 20 sigma vertical layers) provide the most detailed output, but this also goes hand in hand with extensive computation times: a 3 month hindcast may take over a month to run. The model that makes use of the coarse grid and 8 sigma layers is much faster; simulating a four-month period takes around 6 days. Model run time could be optimized by imposing a more representative initial salinity field. In this section we compare the model performance for different model settings.

Figure 3.9 shows that the local grid refinement has some influence on the water levels in Borssele. These are better reproduced in the simulation with horizontal grid refinement. The coarse models estimate the water level elevation during HW within 20-30 cm of the observed water level. All models overestimate the tidal amplitude at Hansweert, no matter the grid size or the number of vertical layers. Increasing the bottom roughness leads to slightly better results. The sensitivity to grid refinement is not fully understood and is subject of current research. At this moment we considered the velocity and water level calibration sufficient for this study.

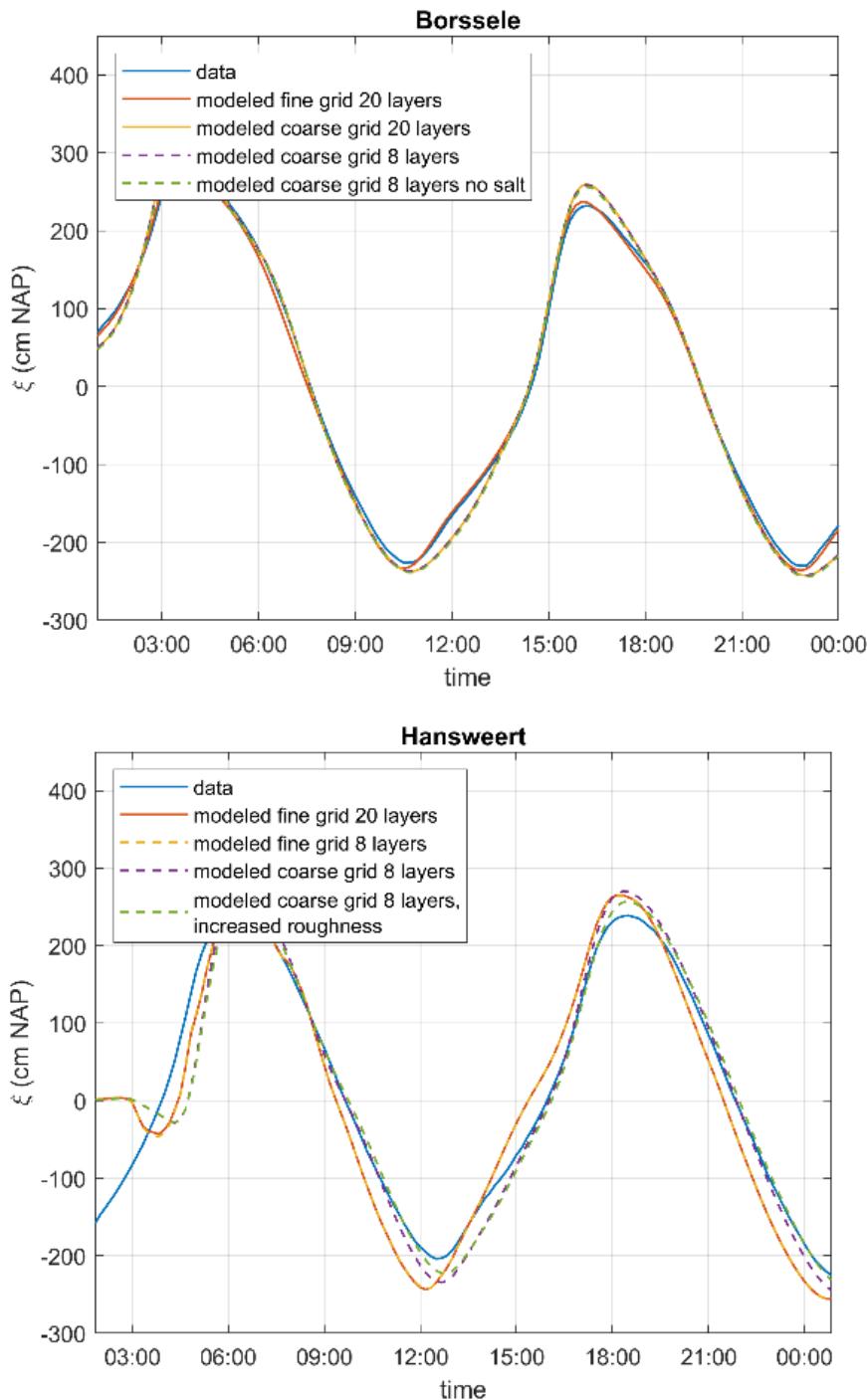


Figure 3.9: Comparison of the simulated water levels at Borssele (top) and Hansweert (bottom).

Since we are mainly interested in the 3D flow patterns in the deep channels, it is essential to validate whether this is reproduced well by all models. The results plotted in Figure 3.10 show that all models lead to comparable flood patterns in m- and n-direction regardless of the grid size and vertical layering.

From the results presented in this section, we conclude that it is sufficient to model the hydrodynamics with a coarse grid and 8 sigma layers. The detailed simulations do not provide new insights that would justify the increased computational time.

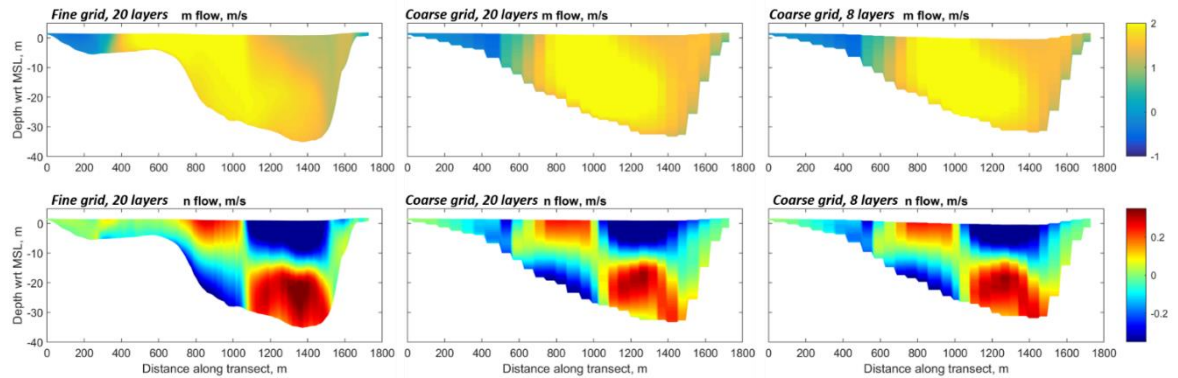


Figure 3.10 The effect of grid refinements on the vertical flow patterns in the primary direction (top) and secondary direction (bottom). Mind that the left panels apply a different bathymetry than the two right panels. The right panels applied the 2011 NEVLA model, whereas the left panel bathymetry was updated based on Vaklodingen data. Remarkably, the general secondary flow patterns do not seem to be significantly influenced by the bathymetry difference. A rerun with equal bathymetry would take 3 months. Also we will do the close analysis of the Hansweert pit based on the 2018 bathymetry.

3.4 Modelling results

3.4.1 3D flow patterns: secondary flow

Both the model results and the ADCP data reveal local circulation cells in n-direction, which contribute to a secondary flow. We use the model simulations to determine the flow patterns across the entire channel. Figure 3.11 we analyze the flow patterns across the pit of Hansweert up to the shoal of Ossensisse. During flood, two circulation cells with opposing direction appear in the channel and one smaller cell is visible in the shallow part. During ebb, we observe a large circulation cell in the deepest part of the channel and a smaller one (with equal direction) in the shallower part south of it. Circulations cells are hardly visible in the shallow part. Note that the absolute flow velocities over the shoal are much higher during ebb than during flood.

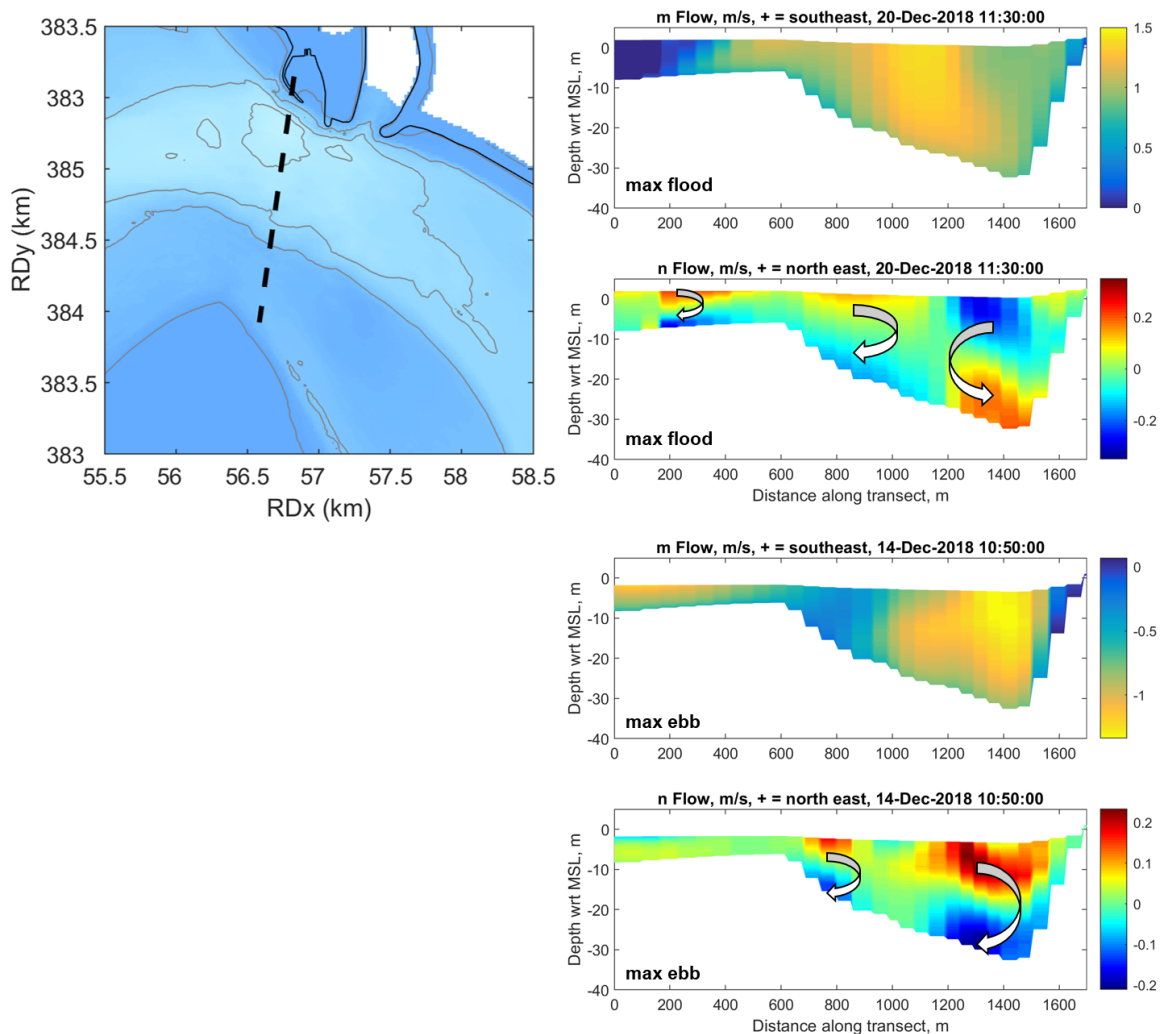


Figure 3.11 Analysis of the flow patterns in Hansweert

Similar to the case in Hansweert, we observe two circulation cells with outward direction at the bed in Borssele during flood (see Figure 3.12). The direction of the circulation cells is opposite during ebb and a small additional cell arises around the -10 m depth contour. Note the significant difference in flow velocities in m-direction during flood (~ 2 m/s) and ebb (~ 1.3 m/s) in the center of the channel, similar to the patterns shown in the data analysis.

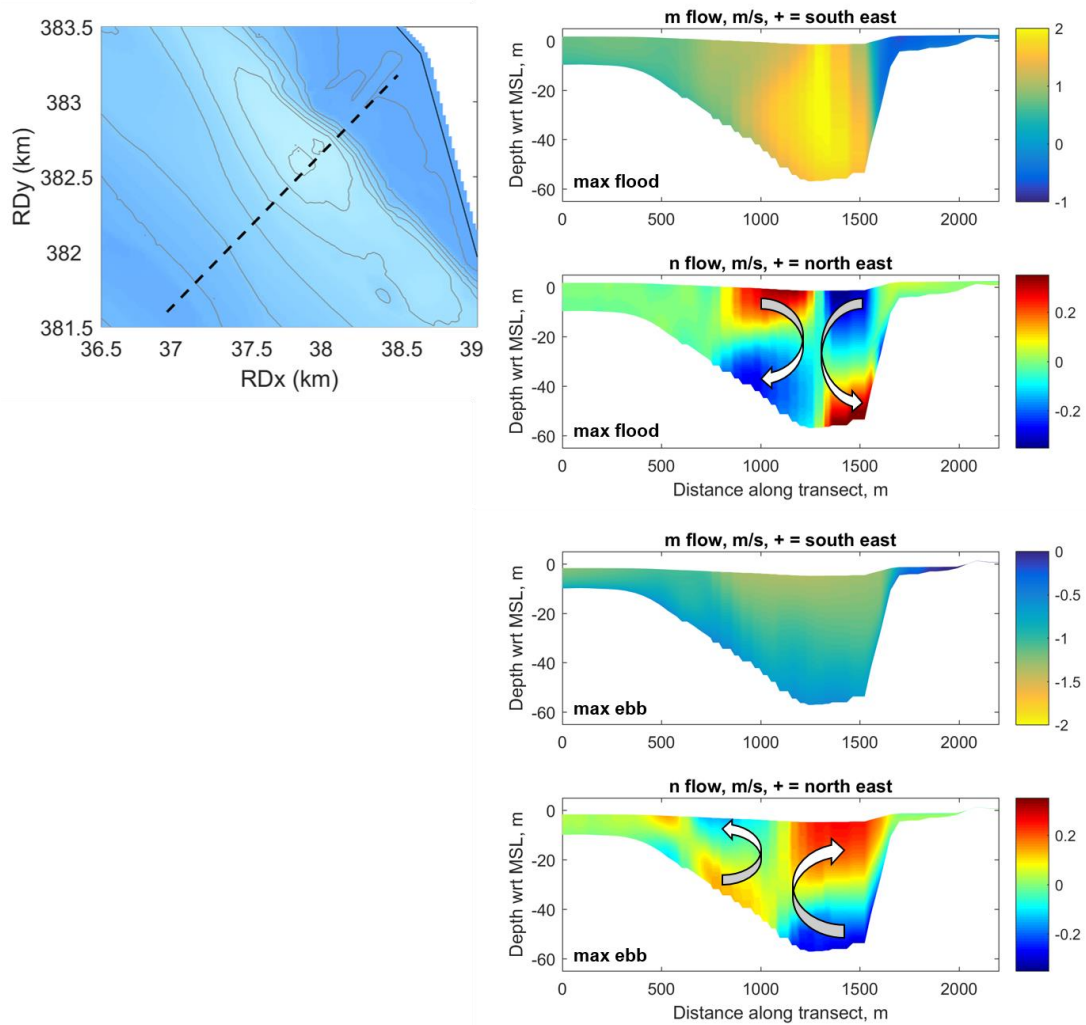


Figure 3.12 Analysis of the flow patterns in Borssele

Figure 3.13 and Figure 3.14 show the flood velocity patterns for Borssele and Hansweert along three consecutive cross-sections (A, B, C and G, H, I respectively). This indicates the spatial variation of the vertical flow. Although the magnitude of the flow velocities remains similar, the flow patterns do vary. This holds in particular for the flow patterns in n-direction in Borssele, where a variation from two to three recirculation cells is noticed over a distance of ~100 m. The flow patterns over the cross-sections in Hansweert remain similar over the observed short distances. However, it is advised to analyze transects that are further away from each other in future studies, since these are expected to be significantly different at the seaward and at the landward side of the pit. These deviations, combined with transport gradients, are likely to be key-factor in the sediment transport from the pits towards the shoals.

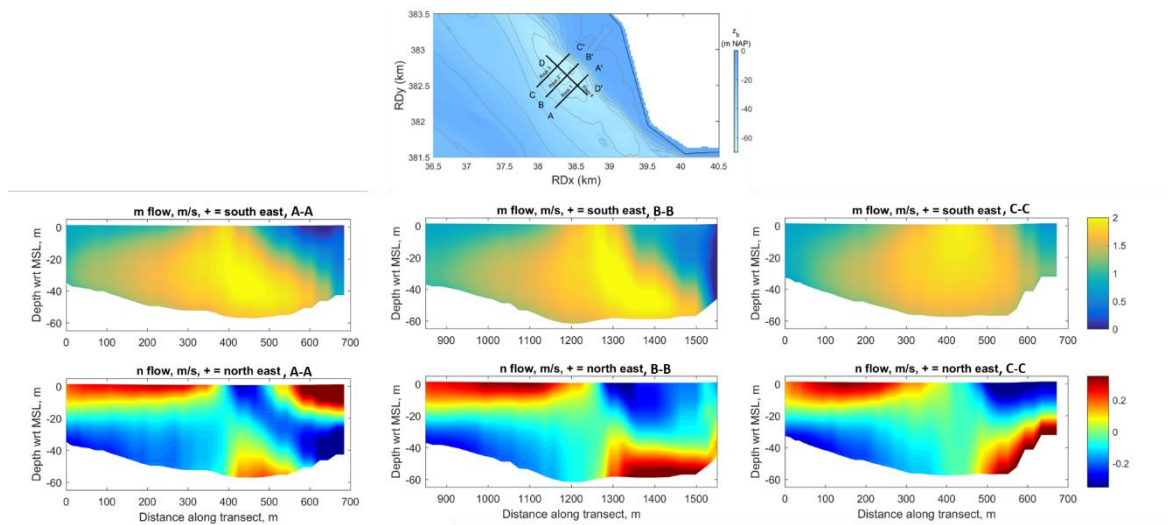


Figure 3.13 Flood flow through three transects in the Borssele Pit

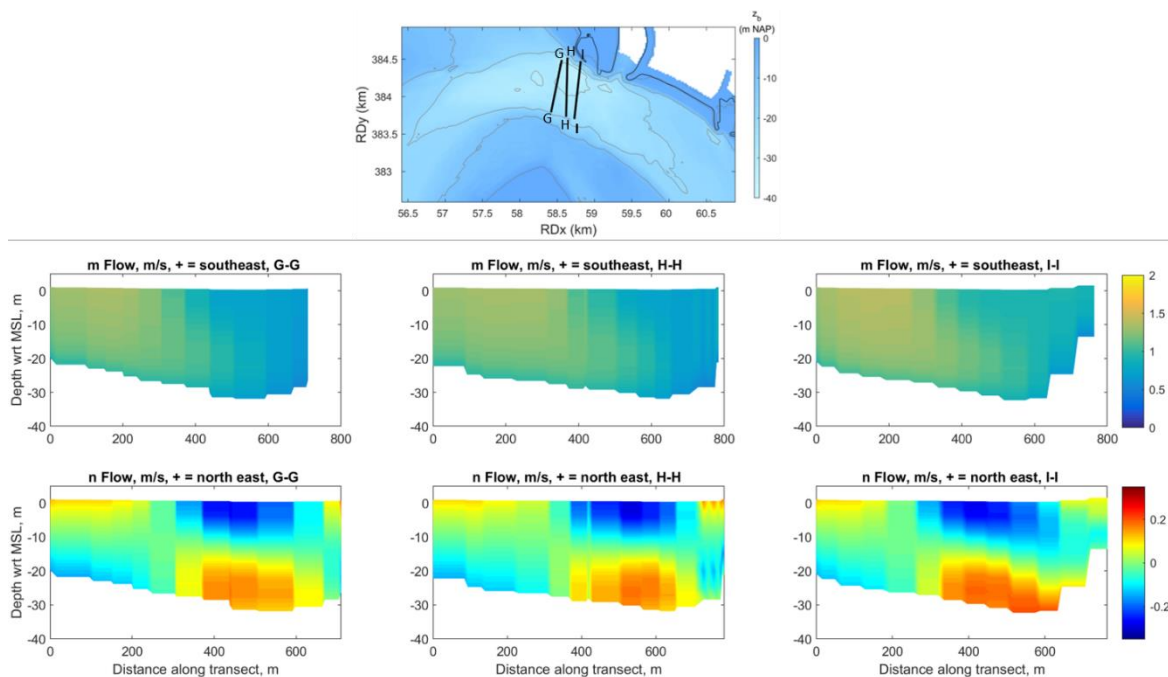


Figure 3.14 Flood flow through three transects in the Hansweert Pit

3.4.2 Process analysis

Both the ADCP data and the model results show that the highest flood flow velocities in m-direction in the channel of Hansweert occur in the inner bend (southern part). Besides, we have observed circulation cells. Combined, these findings suggest the occurrence of a secondary flow from the channel towards the shoal.

The observed patterns in m- and n-direction are not the same for the analyzed locations. Whereas in Borssele we always observe two circulation cells in opposite direction, in Hansweert they have opposite direction during flood, and they are in the same direction during ebb. It seems as if a very small cell separates the two larger cells during ebb, but the flow velocities of this cell are so small that it is likely to be negligible. Consequently, the secondary flow near the bed at the southern edge of the channel is in all cases directed towards the shoal of Ossensisse.

However, it is not only the local flow but mainly the spatial gradients that are important for sediment transport (assuming mainly bed-load). Therefore, we suggest a 2D spatial analysis of the flow just above the bed (near bottom layer in the model) should be performed in order to couple these results to the sediment transport patterns. Note that this analysis should be performed on the flow patterns near the bed computed with a 3D simulation, since large variation in flow patterns are observed over the water column.

To identify the potential causes of the secondary flow, a simulation is performed excluding salinity. The results of the simulation with and without salinity are shown in Figure 3.15 for Borssele and in Figure 3.16 for Hansweert. We observe that the circulation cells in n-direction at Borssele disappear when neglecting salt-effects, while they are still visible – although much weaker- in Hansweert. From this, we hypothesize that the secondary flow in Borssele is probably primarily caused by density differences, while the secondary flow in Hansweert is likely to be an effect of the channel bend itself. A 'bend' shape of the pit and its' surrounding is also more pronounced at Hansweert than at Borssele.

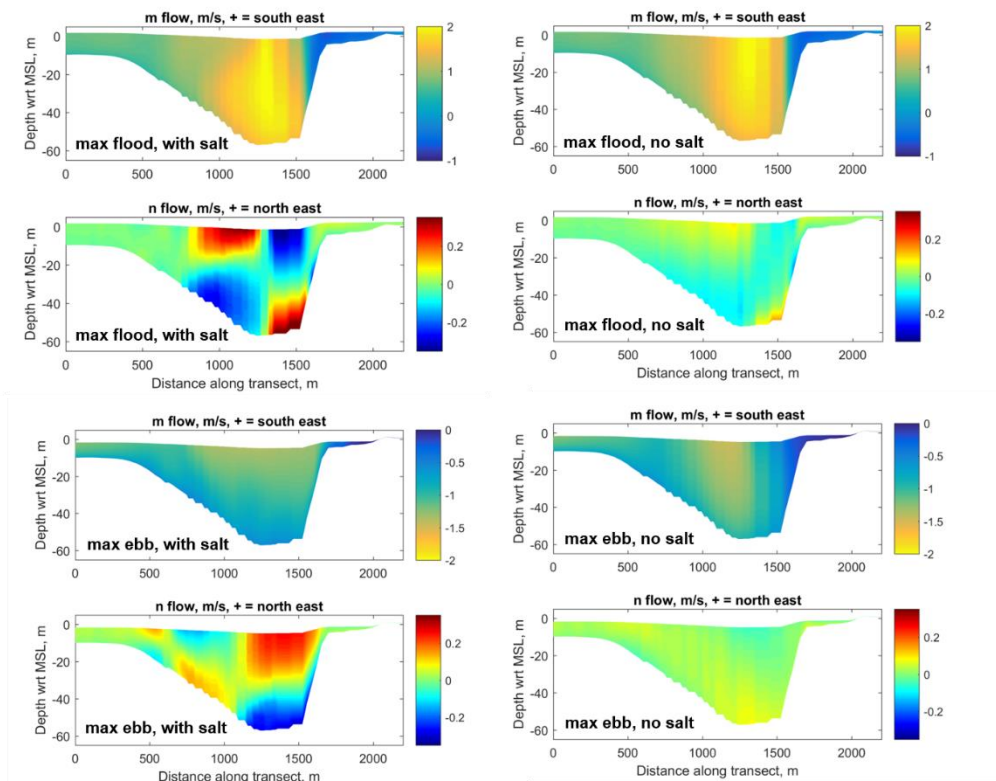


Figure 3.15 Comparison of simulation results with salt (left) and without salt (right) at Borssele

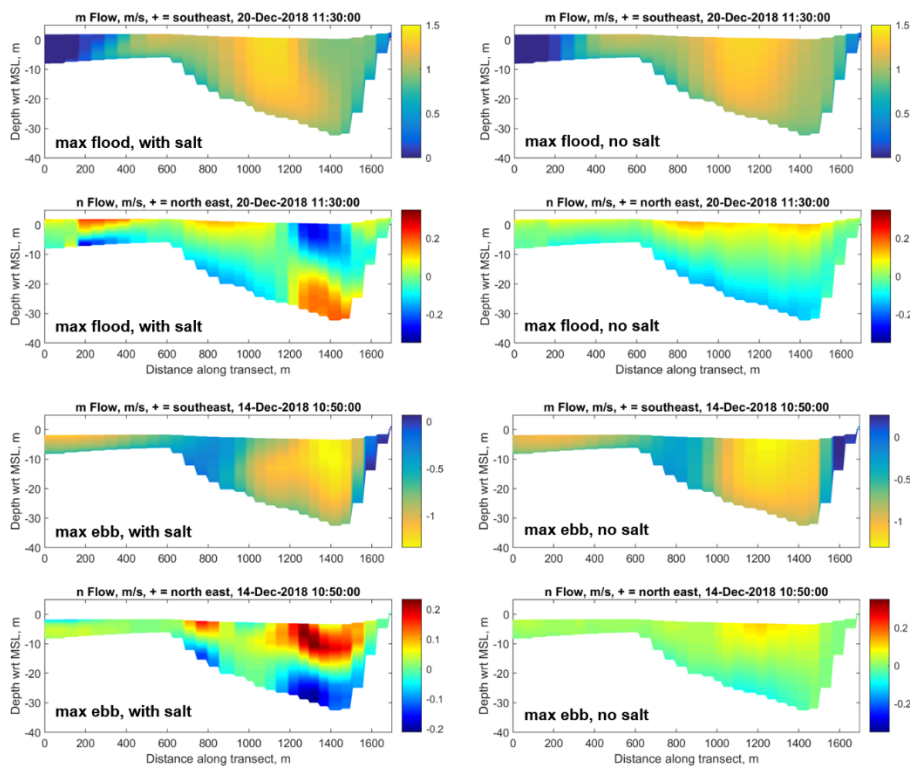


Figure 3.16 Comparison of simulation results with salt (left) and without salt (right) at Hansweert

4 Discussion

4.1 Comparison to traditional river bend flow

Traditional river bend flow leads to elevated water levels in the outer bend and a secondary flow directed inward near the bed and outward at the surface. Our results deviate considerably from this traditional concept. We observe and model multiple circulation cells in a cross-section. Part of these cells are in line with traditional bend flow theory (outward at the surface, inward near the bed), but part of these cells contradicts the theory. This requires a closer analysis of governing processes.

3D Modeling (Figure 3.15 and Figure 3.16) shows that salinity gradients play a major role in the secondary flow dynamics, in terms of magnitude, in terms of secondary flow direction and in terms of number of circulations cells. For example, the secondary flow magnitudes are much larger in the presence of salinity gradients, secondary flow direction reverses from peak ebb to peak flood at Borssele and three secondary flow cells develop instead of one at maximum flood at Hansweert. However, the model was not validated for salt. Very limited data of salinity are available covering only short periods of time or only fixed locations, whereas salinity profiles across the transects measured would be needed for relevant model validation.

Apart from salinity gradients, other factors may be important as well for the observed circulation flows. The shallow morphology and plan form near the breakwaters at Borssele may influence circulations patterns. The breakwaters will induce horizontal vortices. For example, low velocities towards the northern shore in Figure 2.9 and Figure 2.8 may be interpreted as influence of the breakwaters. Another factor potentially responsible for these flow disturbances relates to cooling water released at the location of the breakwaters. This cooling water can generate local density flows due to the difference in temperature and density. However, these temperature driven flows are not included in our model.

The tidally varying, bi-directional flow is more complex than unidirectional, relatively constant river flow. In an estuarine case study like in the current study, channel dimensions are the result of both ebb and flood flows so that the dimensions do not ideally fit each of the ebb or flood flow. Flooding and drying of shoals occur at different stages during the tide and can have an important impact on peak flood and ebb flow patterns including secondary flow dynamics. Also, the channel morphology landward and seaward from the pit will have a large impact on how flow occurs in the pits.

This study focused on the secondary flow dynamics at peak ebb flow and peak flood flow since measurements were available to compare with. Future study may focus on analyzing in more detail the modeled intratidal secondary flow dynamics. Such a study could explore the typical adaptation timescale and coherence of the secondary flow.

Our study suggests that schematizations to parametrize secondary flow in 2D (that exist in Delft3D) are not suited to represent secondary flow dynamics found in the pits at Borssele and Hansweert where salinity gradients and a complex plan form and bathymetry are present.

4.2 Analysis of governing processes

In order to study the processes governing the secondary flow dynamics we now analyze in more detail the contribution of different terms in the secondary momentum equation.

The imbalance in the secondary momentum equation is defined by subtracting a depth-average of the Reynolds averaged form of the secondary momentum equation under hydrostatic and Boussinesq approximation (Nidzieko et al., 2009) and is given by:

$$\begin{aligned} \frac{\partial u_n}{\partial t} = & \frac{u_s^2 - \overline{u_s^2}}{R_s} - \left(u_s \frac{\partial u_n}{\partial s} - \overline{u_s \frac{\partial u_n}{\partial s}} \right) - \frac{g}{\rho_0} \left(\int_z^0 \frac{\partial \rho'(z')}{\partial n} dz' - \overline{\int_z^0 \frac{\partial \rho'(z')}{\partial n} dz'} \right) \\ & - f \left(u_s - \overline{u_s} \right) - \left(\frac{\partial \langle u_n u_z \rangle}{\partial z} - \frac{\tau_{b,n}}{\rho H} \right). \end{aligned} \quad (1.1)$$

Here, a natural coordinate system s, n, z is used, where s is the primary flow direction, n the direction perpendicular to the primary flow direction and z the vertical direction. Furthermore, u_s, u_n are the velocity components in s, n direction in m/s, respectively, R_s is the radius of curvature of the channel bend in m, g is a gravitational constant with value 9.81 m/s^2 , ρ_0 is the mean background density of the water in kg/m^3 , ρ' are density deviations from the mean value, f is the Coriolis parameter, $\tau_{b,n}$ is the bed shear stress in n direction and H is the flow depth (about 60m for Borssele and about 30 m for Hansweert). The overbar denotes a depth-averaging operation, whereas $\langle \dots \rangle$ denotes a time-averaging operation.

A scaling analysis reveals the order of magnitude of the separate terms a priori. The horizontal velocity scale is chosen as $u_s, u_n \sim U, V$, where it is assumed that the secondary velocity is a fraction of the streamwise velocity, that is, $V \approx \alpha U$ with α a constant between 0 and 1. The velocity U itself is of $O(10^0)$. A horizontal length scale $s, n \sim L$, where L is any appropriate horizontal distance, like the channel width or the length of the pit. A time scale $t \sim T$, where T is the tidal period is defined. The radius of curvature is about 10 km for Borssele and 1 km for Hansweert. Using these, the order of magnitude of the terms may be evaluated.

- $\left(\frac{\partial u_n}{\partial t} \right) \propto \frac{\alpha U}{T} \approx O(10^{-6})$
- It is assumed that the primary flow is relatively uniform over the depth, that is, deviations from the mean are not too large ($< \sim 10\%$), yielding: $\frac{u_s^2 - \overline{u_s^2}}{R_s} \propto \frac{\gamma U^2}{R_s}$, with $\gamma \approx O(10^{-1})$. Then $\frac{\gamma U^2}{R_s} \approx O(10^{-5})$ for Borssele and an order larger for Hansweert.
- $\left(u_s \frac{\partial u_n}{\partial s} - \overline{u_s \frac{\partial u_n}{\partial s}} \right) \propto \left(\frac{\alpha U^2}{L} - \gamma \frac{\alpha U^2}{L} \right) \approx O(10^{-3}) - O(10^{-4})$, where we have chosen $L \approx O(10^3)$, which is roughly the order of magnitude of the pit. There is some sensitivity in the choice of this parameter.
- $-g/\rho_0 \approx O(10^{-2})$, assuming $g = 9.81 \text{ m/s}^2$ and $\rho \approx 1030 \text{ kg/m}^3$. It is assumed that density fluctuations ρ' are of $O(10^1)$, such that $\int_z^0 \partial \rho' / \partial n dz' \approx \rho' H / B \approx O(10^{-1}) - O(10^{-2})$ with width B is of $O(10^3) - O(10^4)$. Multiplying this by g/ρ then yields that the baroclinic pressure gradient term is roughly of $O(10^{-3}) - O(10^{-4})$
- $f(u_s - \overline{u_s}) \propto f \alpha U \approx O(10^{-5})$

- We assume a linearized friction that is defined through $\tau_{b,n} = \rho c_f V^2$. We assume that the turbulent velocity fluctuations can be defined through $u' = rU$, where r is a constant of $O(10^{-1})$. Then $\left(\frac{\partial(u'_n u'_z)}{\partial z} - \frac{\tau_{b,n}}{\rho H}\right) \propto \frac{r^2 U^2}{H} - \frac{\rho c_f V^2}{\rho H}$. In field situations $c_f \approx O(10^{-3})$, thus the friction term is roughly of $O(10^{-3})$.

The relative importance of each term is listed in Table 4.1. A rough scaling analysis shows that it can be expected that the phenomena are dominated by the balance between the baroclinic pressure gradient, advective acceleration and friction.

Table 4.1: Overview of the relative importance of each term in Equation 1.

Term	Order of magnitude
Inertia	$O(10^{-6})$
Centrifugal acceleration	$BS: O(10^{-5}), HW: O(10^{-4})$
Advective acceleration	$O(10^{-3}) - O(10^{-4})$
Baroclinic pressure gradient	$O(10^{-3}) - O(10^{-4}), Bo > HW$
Coriolis	$O(10^{-5})$
Friction	$O(10^{-3})$

We used Delft3D FM to quantify the terms described in equation 1.1. That exercise quantified the local values and variations of all terms over the transects. The right- and left-hand terms of equation 1.1 should be equal, but it appeared to be difficult to derive this through quantifying by Delft3D results. Summation of the right-hand side was not even like the inertia term of the left-hand side. A possible explanation for this shortcoming is that our model applies a curvilinear grid that requires correction terms in the momentum equation that we did not consider in our analysis. Also, small errors due to linearization of values across a cell with respect to the location of observation points may have contributed to the limited accuracy. Finally, we did not consider vertical velocities that will have an impact as well.

Still, quantifications of the terms by Delft3D FM showed that the inertia term, the baroclinic pressure gradient term and the friction terms were dominant across the cross-section. This is in line with the scaling analysis described before, except for inertia versus advective acceleration. This suggests that secondary circulations at the Borssele pit are driven predominantly by salinity differences and friction effects.

4.3 Possible impact on sediment transport

The larger framework of this study encompasses an investigation of the transport pathways of sediment in the deep pits of the Western Scheldt. A major question thus relates to the potential impact of the observed and modeled secondary flow on the sediment transports. Some general remarks are made in this respect:

- Flood flows are dominant in transporting sediments, because ebb primary flows in the pits of Borssele and Hansweert are notably smaller than flood flows and so are the gradients in flow magnitude. Flood flows will thus probably transport more sediments. In addition, gravitational circulation causes largest flood flows to be subsurface in contrast to maximum ebb flows that occurs at the water surface. Since sediment concentrations are larger at larger depths, this enhances residual landward sediment transport. Further study should reveal where the largest tide-residual sediment

transport gradients are located. These gradients determine the morphodynamic development and may explain the observed depth of the deep pits.

- The secondary flows are typically an order of magnitude smaller than the primary flows. This suggests that the impact on the sediment transport magnitude is limited but that there may still be a relevant impact on the direction of the sediment transport.
- The observed and modeled secondary flow patterns can influence sediment transport in two ways. First, the secondary flow will impact on the direction and magnitude of the bed load transport. Secondly, the secondary flows enhance mixing of suspended sediments in the water column. Whether this leads to higher concentrations or larger transports (or not) is subject of future research.
- The effect of secondary flow on lateral bed load sediment transport in the Borssele pit seem to cancel out over the ebb and flood stage of the tide (i.e. show similar patterns with opposite secondary flow directions).
- In contrast, other locations such as the shallower part of the Hansweert pit cross-section have a continuous inward directed (towards the southern shoal) secondary flow near the bed, independent of the tidal phase. This suggests the development of a tide residual bed load transport up-slope towards the shoal during a tidal cycle. This aligns with the perceived transport of sediment towards the inner bend after two test disposals of dredged sediment in the Put van Hansweert (Deltares, 2018).
- Salinity gradients are one of the governing drivers of secondary flow in the Western Scheldt. Sediment transports by secondary flow in the pits cannot be derived from 2DH models with parametrized bend flow dynamics. The effects of gravitational circulation can only be resolved in 3D models.

5 Conclusions

This study investigated the presence of secondary flow patterns in two Western Scheldt pits by analysis of field data and numerical model simulations, as well as their potential impact on the transport of sediments in these pits by expert judgement. Observations and model studies showed the existence and magnitude of the secondary flows. Small salinity gradients appeared to be important drivers of the secondary flows.

We can now answer the research questions formulated at the start of this study.

What are prevailing 3D flow patterns in the pits of Borssele and Hansweert?

The analysis of ADCP measurements in the pits of Borssele and Hansweert shows that peak ebb flows are smaller and are laterally more uniformly distributed across the cross section than peak flood velocities. The analysis also reveals other significant 3D flow patterns in both pits. These include:

- secondary currents with values of about 10% of the primary flow at peak ebb or flood.
- secondary currents appear in multiple circulation cells over the measured transects.
- characteristics of gravitational circulation are present during peak ebb and flood flows; ebb flows have largest velocities at the surface linearly decaying vertically, while flood flows show a subsurface, near bed maximum velocity.

Can these flow patterns be modeled by a 3D hydrodynamic model (Delft3D FM)?

It appears that a relatively coarse grid (50x200 m²) with 8 sigma layers and standard hydrodynamic parameter settings is enough to reproduce the observed 3D flow patterns. Analyzing transects longer than the observed transects shows even more recirculation cells across a cross-section. Model run time is relatively long, namely about 6 days covering about 3 months including a necessary spin-up of the salinity field.

What are the processes responsible for the 3D flow patterns?

Model sensitivity analysis enabled us to explore the mechanisms governing the secondary flow dynamics. Runs applying a uniform density (no differences in salinity) shows that

- the secondary flows are much weaker in case of a uniform density,
- circulation cell flow direction may reverse,
- circulation cell location and size change and
- the number of circulation cells may change.

A rough scaling analysis of the different terms in the lateral momentum equation shows that the driving mechanisms of the circulation patterns probably consist of the baroclinic pressure gradient, advective acceleration and friction. This is confirmed by quantification of the lateral momentum balance terms by Delft3D FM output across the transects. However, the Delft3D FM quantification did not lead to a closed system (right- and left-hand side of the equation where not equal). This is probably caused by small errors arising from the application of a curvilinear grid and the interpolation of cell-based model results on model output points (observation points). Still, the current model was not validated for salinity because of limited data availability. We recommend including salinity measurements in future transect measurements.

What are the potential implications of these flow patterns on the transport of sediment deposited in the pits by dredging activities?

The secondary flow patterns probably do not have a large impact on the total amount of transported sediment, since their magnitude (max.~0.3 m/s) remains small compared to the primary flows (max.~2 m/s). However, the secondary flows may have an impact by enhanced mixing of suspended sediments in the water column and may influence suspended sediment concentrations and transports. Furthermore, the direction of the sediment bedload transport is affected by the secondary circulations. The circulation cells often reverse from ebb to flood, but some locations at Hansweert face a continuous (independent of the tidal phase), up-slope circulation flow near the bed in southern direction of about 0.2 m/s. That flow will result in a tide-residual transport of sediment from the deepest part of the pit towards the southern shoal adjacent to the pit. This aligns with the perceived transport of sediment towards the inner bend after two dredged-sediment dumps in the Put van Hansweert (Deltares, 2018).

6 Referenties

Deltares, 2018. Baggerdepositie in diepe geulen. Strategie voor het plaatsen van gebaggerd materiaal in de diepere getijdegeulen van de Westerschelde. Deltares rapport 1210301-000-ZKS-0027. Opdrachtgever Vlaams Nederlandse Schelde Commissie. Auteurs : Bas Huisman, Reinier Schrijvershof, Thijs Lanckriet en Jebbe van der Werf.

Plancke, Y., Claeys, S., Verwaest, T., Mostaert, F., 2017. Overleg Flexibel Storten: Deelrapport 23 – Stroming- en sedimentmeting ter hoogte van de diepe put van Hansweert. Versie 3.0. WL Rapporten, 00_031_23. Waterbouwkundig Laboratorium: Antwerpen.

Schrijver M. , J van het Westende, 2011, Stroommeting Put van Borssele. Rijkswaterstaat Zeeland, Meetadviesdienst. Rapportnr. 0542S/ZHHW-2011-10, Middelburg, oktober 2011
Rijkswaterstaat CIV, 2018. Personal communication.

Tiessen, M., Vroom, J. & van der Werf, J., 2016. *Ontwikkeling van het Delft3D FM NeVla model voor het Schelde estuarium-Waterbeweging in de Westerschelde en stroming over de plaat van Walsoorden*. 1220095-000-ZKS-0023, Delft: Deltares.

Vroom J., de Vet P., van der Werf J. (2015) Validatie waterbeweging Delft3D-NeVla model Westerscheldemonding. Deltares rapport 1210301-001-ZKS-0001

A Validation additional transects Borssele

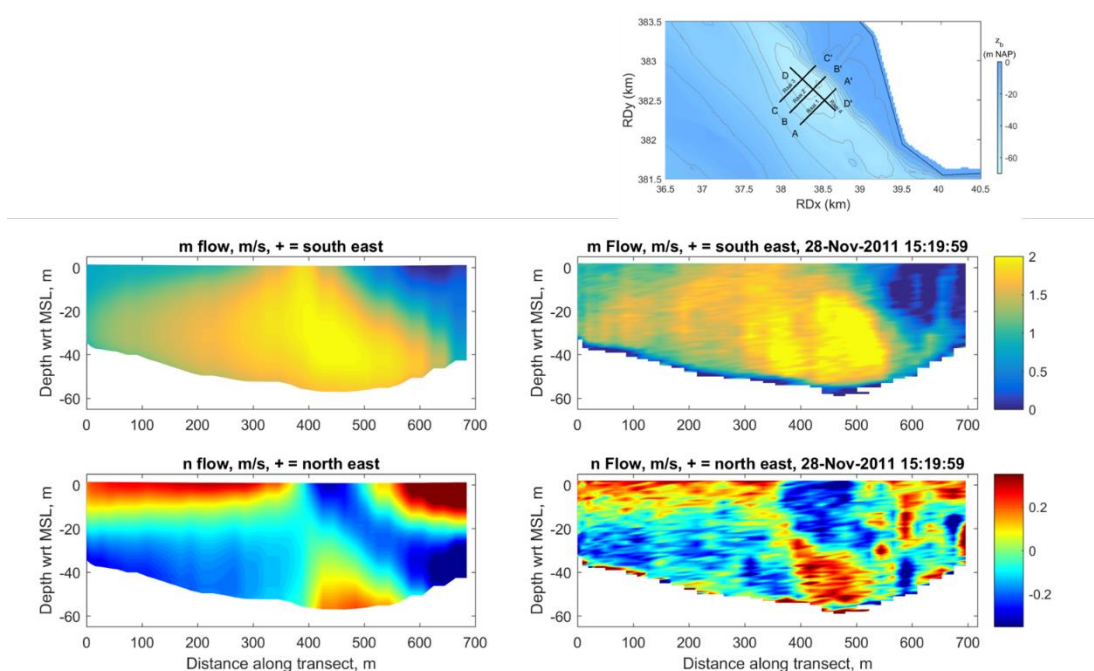


Figure A.1 Transect A-A' during flood, model results (left) and data (right).

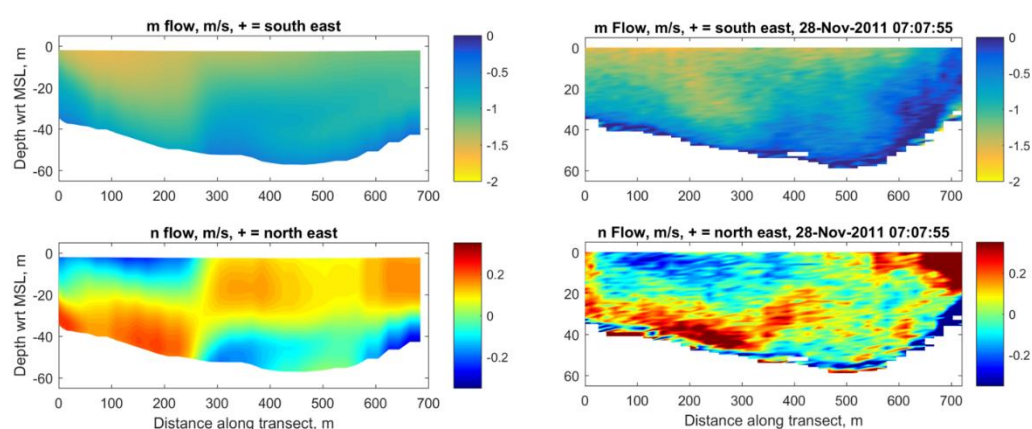


Figure A.2 Transect A-A' during ebb, model results (left) and data (right).

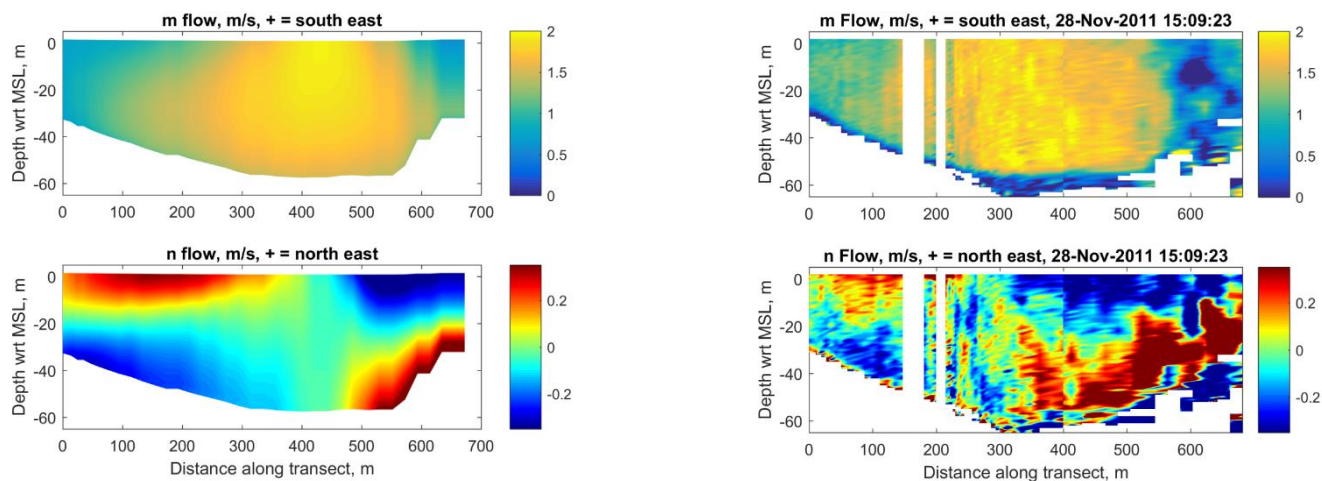


Figure A.3 Transect C-C' during flood, model results (left) and data (right).

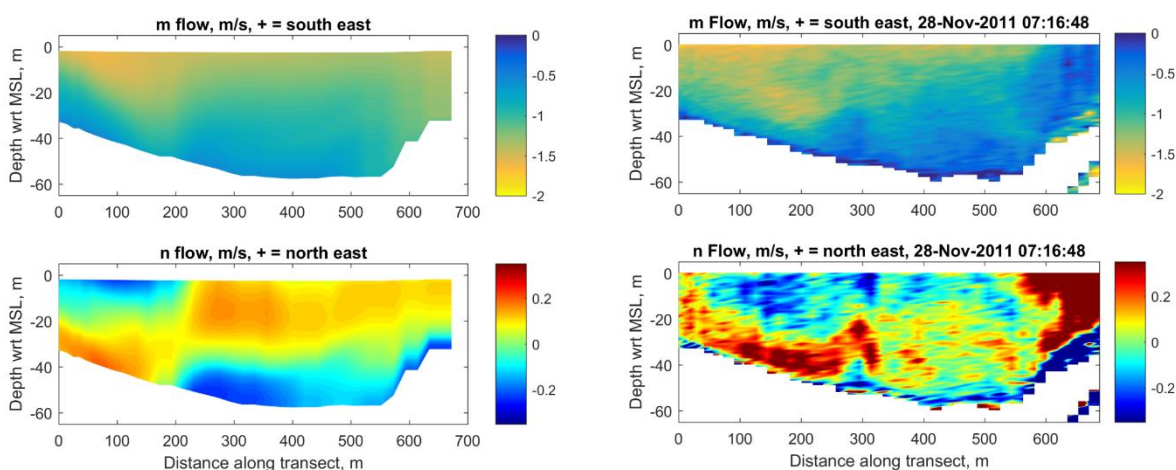


Figure A.4 Transect C-C' during ebb, model results (left) and data (right).

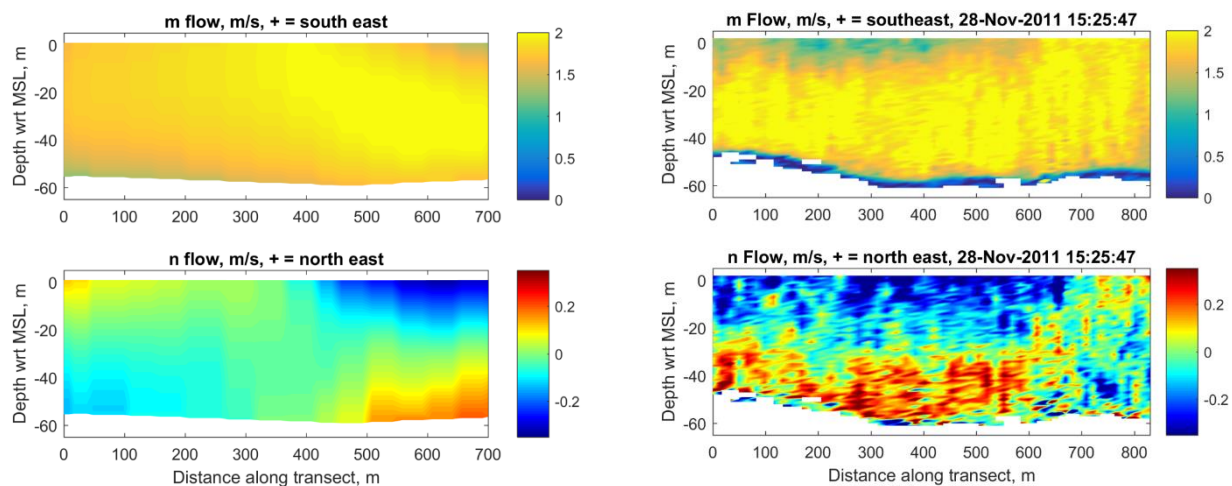


Figure A.5 Transect D-D' during flood, model results (left) and data (right).

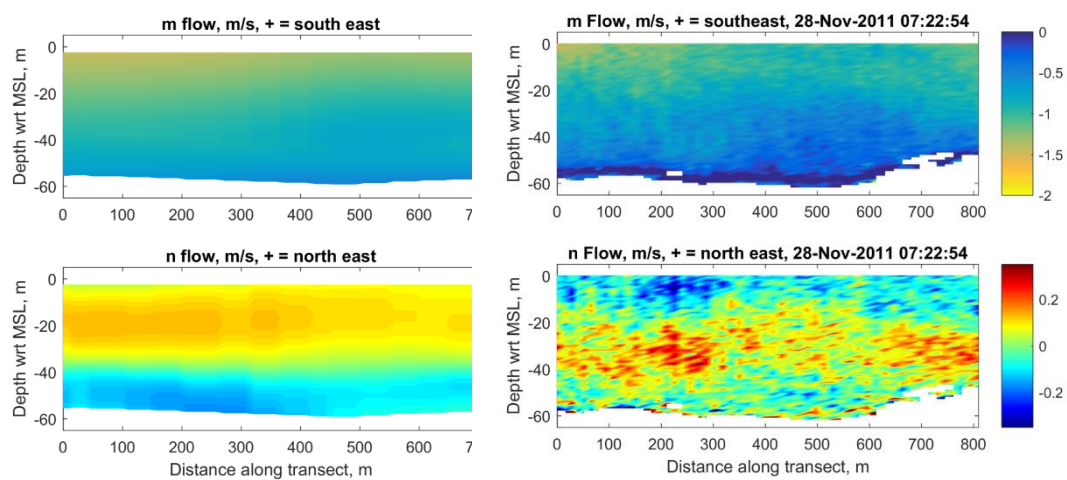


Figure A.6 Transect D-D' during ebb, model results (left) and data (right).

B Velocity profile validation over depth

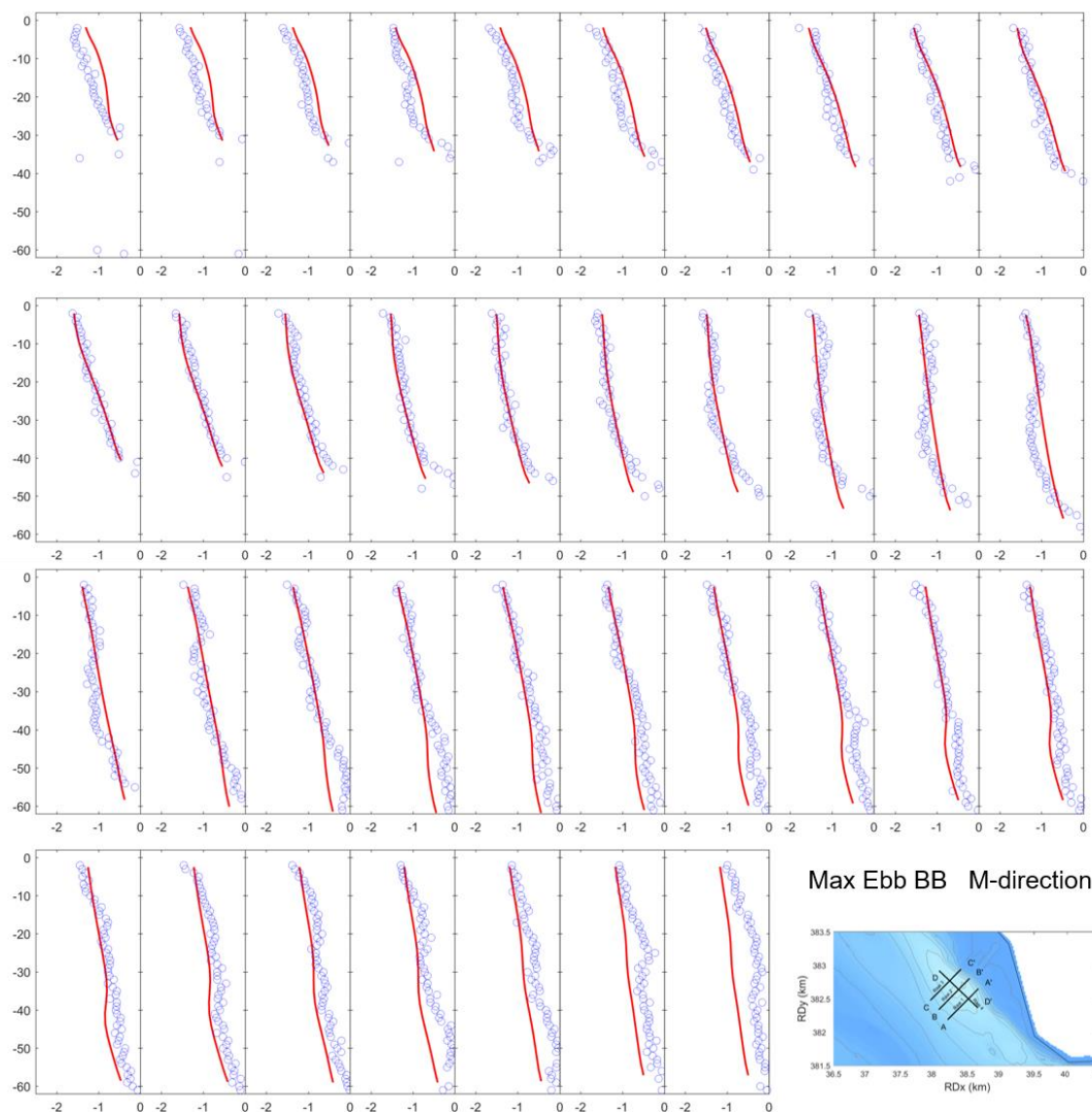


Figure B.1 Velocity profiles in M-direction, transect BB during maximum ebb

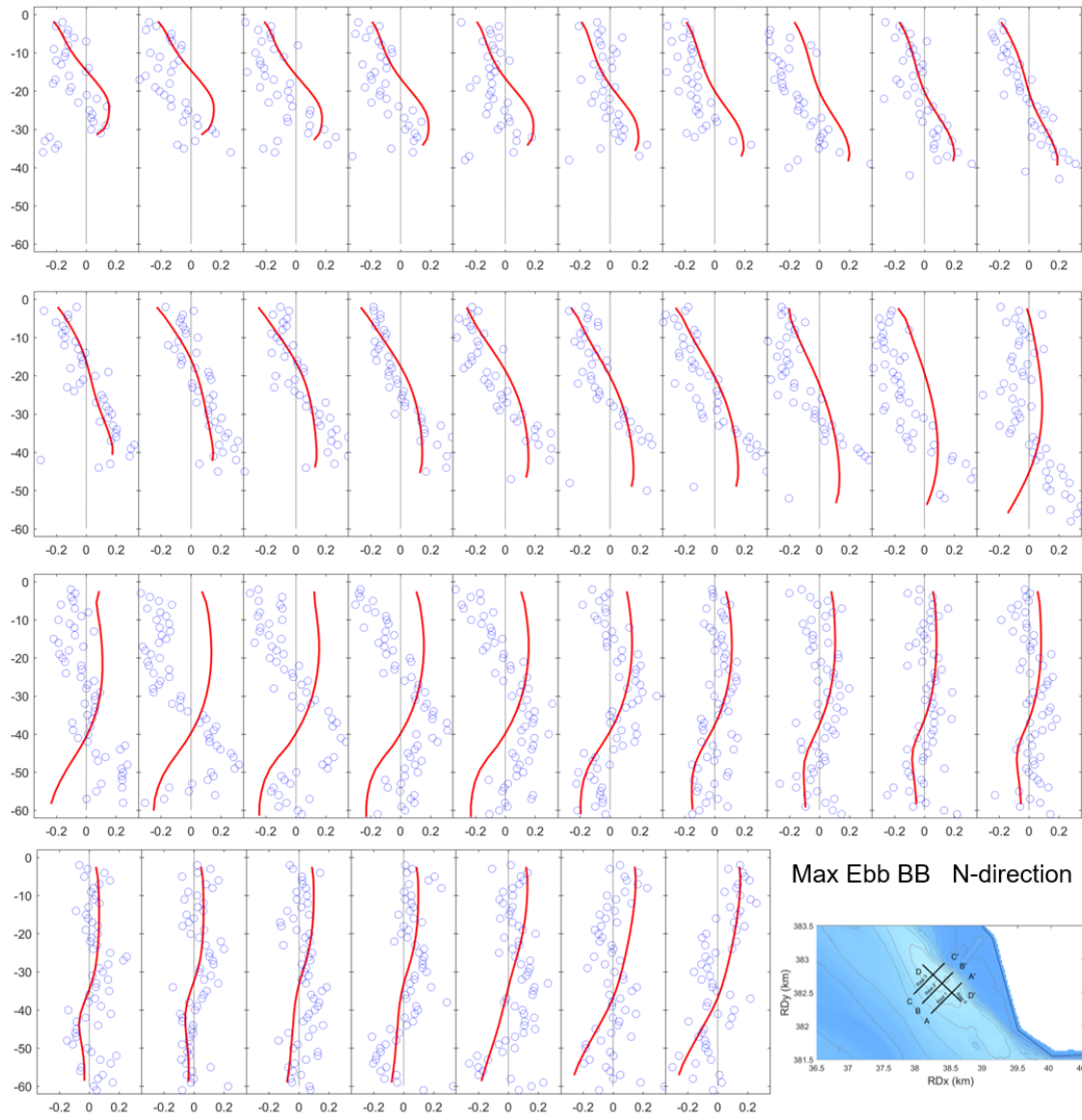


Figure B.2 Velocity profiles in N-direction, transect BB during maximum ebb

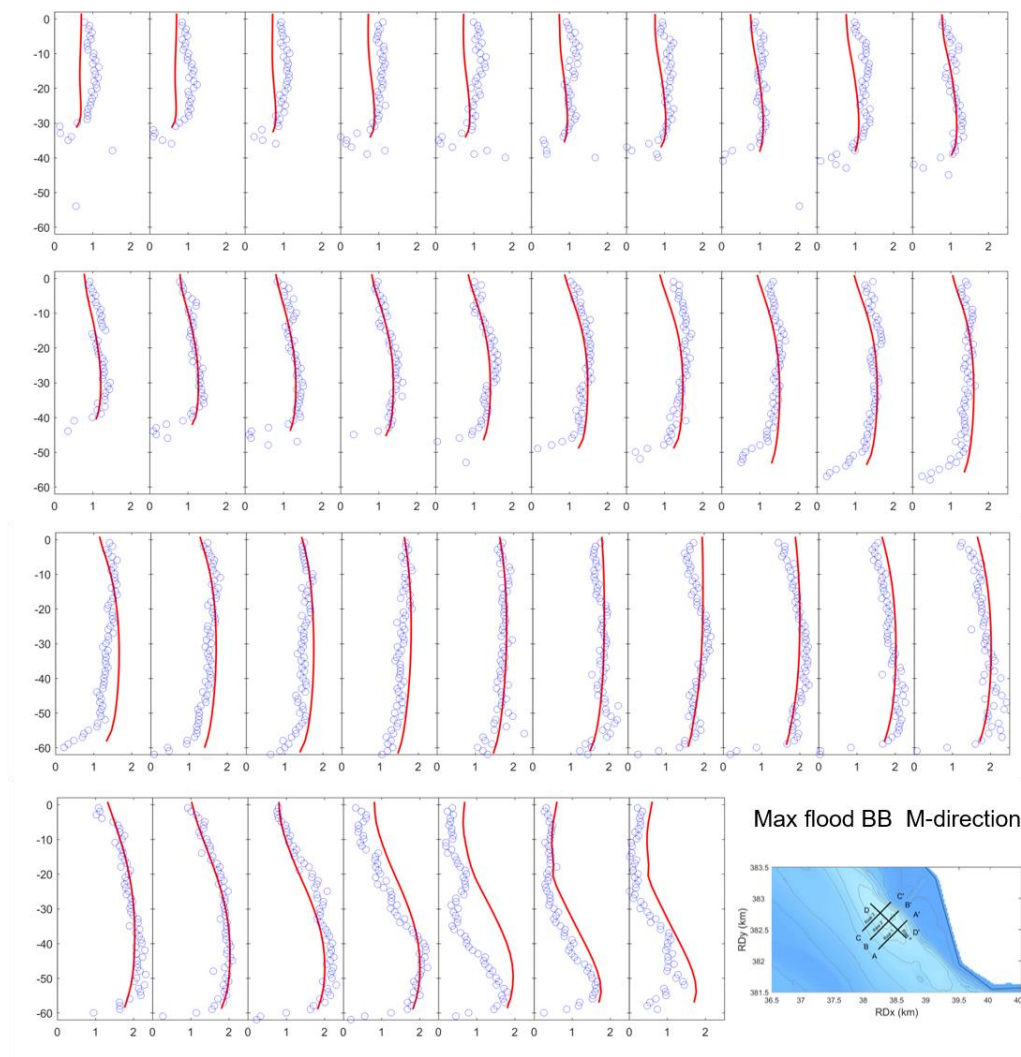


Figure B.3 Velocity profiles in M-direction, transect BB during maximum flood

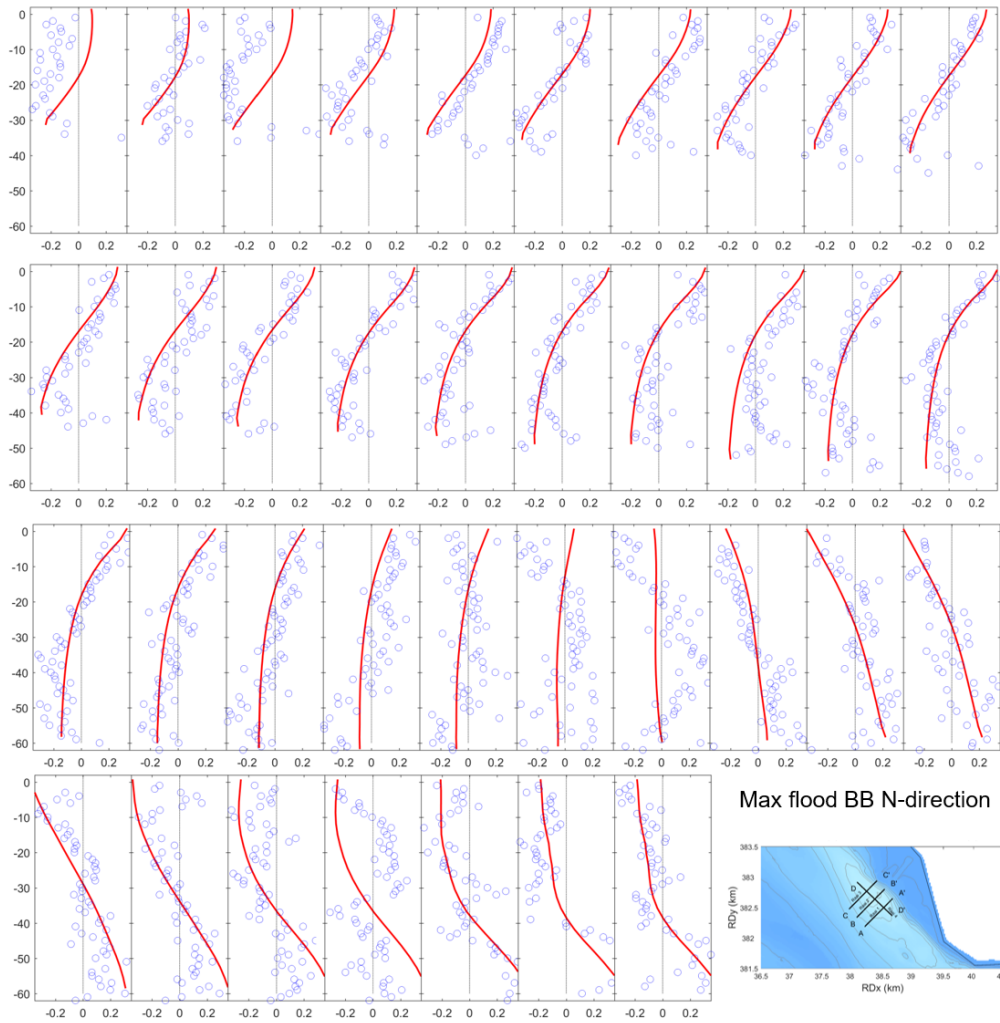


Figure B.4 Velocity profiles in N-direction, transect BB during maximum flood